THE ASTRONOMICAL JOURNAL VOLUME 97, NUMBER 1 JANUARY 1989

THE STELLAR CONTENT OF TWO OB ASSOCIATIONS IN THE LMC: LH 117 (NGC 2122) AND LH 118

PHILIP MASSEY[a]
Kitt Peak National Observatory, National Optical Astronomy Observatories,[b] P. O. Box 26732, Tucson, Arizona 85726-6732

CATHARINE D. GARMANY[a]
Joint Institute for Laboratory Astrophysics, University of Colorado, Boulder, Colorado 80309-0440

MARIABETH SILKEY
Kitt Peak National Observatory, National Optical Astronomy Observatories,[b] P. O. Box 26732, Tucson, Arizona 85726-6732

KATHLEEN DEGIOIA-EASTWOOD[a]
Department of Physics and Astronomy, Northern Arizona University, Flagstaff, Arizona 86011-6010
Received 18 August 1988; revised 27 September 1988

ABSTRACT

Using CCD photometry and digital spectroscopy, we have investigated the stellar content of these two adjacent OB associations in the LMC. We discuss in some depth the details of our CCD photometry since we will be using the same methods to study other Magellanic Cloud associations. We find that these associations contain about 50 stars more massive than $10\mathcal{M}_\odot$. We have spectra for nearly all the members more massive than $15\mathcal{M}_\odot$, allowing placement on a theoretical H–R diagram. Most of the association members lie near the ZAMS, but our spectroscopy has tentatively confirmed two red supergiants. These, and the previously known LH 117 B2 I supergiant, must be of lower mass than several of the unevolved massive members of these associations, implying that these supergiants formed earlier than the majority of the association members by about 6 to 10 million years. We derive an IMF for the associations, finding a slope similar to what is known for massive stars within a few kiloparsecs of the Sun. The Hα luminosity of the associated DEM 323 H II region reported by Kennicutt and Hodge is about a factor of 2 lower than should be produced by the stellar Lyman-continuum flux from stars, suggesting that either the nebulosity is density bounded and/or that the Lyman photons are lost to dust absorption.

I. INTRODUCTION

Two recent studies (Conti, Garmany, and Massey 1986; Garmany, Conti, and Massey 1987) have presented spectral classification for several hundred O and early B stars in the Magellanic Clouds. The ultimate aim of these studies is to directly determine the initial mass function (IMF) and star-formation rate (SFR) for massive stars in the Clouds. When we began this work, it was our intention simply to sample the stars with *UBV* photometry in the literature, but it quickly became apparent that stars in H II regions and crowded OB associations were selectively ignored in such lists. Thus, our spectroscopic studies have so far been concentrated primarily on the field stars in these two galaxies. Nevertheless, it is in these regions without photometry that much of the action occurs: Conti, Garmany, and Massey (1986) did find many early O stars by "fishing" in several of the OB associations cataloged by Lucke and Hodge (1970), using Lucke's (1972) *BV* photographic photometry as a starting point.

Massey (1985) has emphasized that *UBV* photometry and the resulting luminosity functions cannot be used to accurately assess the massive-star population of a region. This is basically due to the degeneracy in colors of stars hotter than 30 000 K. This can be seen graphically by the overlap of O stars (even early O stars) with B stars in the two-color diagrams of Conti, Garmany, and Massey (1986). Nevertheless, color information—and particularly $U-B$ color information—is needed to select which stars need to be observed spectroscopically. At latter spectral types the degeneracy in the $(U-B)$, $(B-V)$ plane is removed, and photometry alone yields adequate information for stars <10–$15\mathcal{M}_\odot$ (i.e., later than about B0.5 V).

Accordingly, we have undertaken a comprehensive program of CCD *UBV* photometry of most of the populous OB associations in both the LMC and SMC. The use of a CCD for photometry avoids much of the difficulty in observing stars within nebulosity, as sky can be determined locally and hence nebular emission will affect the photometry only if it varies on the spatial scale of a few arcseconds. In addition, of course, many stars can be measured at once. However, the principal advantage of the CCD is in the relative ease with which crowding can be dealt with, by using such crowded-field photometry programs as DAOPHOT (Stetson 1987).

In this paper, we present photometry for stars in two adjacent OB associations in the LMC, numbers 117 and 118 in the list of Lucke and Hodge (1970). In addition, we have obtained spectroscopy of the bluest and reddest stars in these fields, and we can use these spectral types to directly determine the massive-star content of these two associations.

II. OBSERVATIONS AND REDUCTIONS

a) Photometry

All *UBV* observations for this project were obtained during nine beautiful, photometric nights in late November and early December 1985 using the CTIO 0.9 m and an RCA CCD (RCA4). The filters used were the standard Kitt Peak

[a] Visiting Astronomer, Cerro Tololo Inter-American Observatory, National Optical Astronomy Observatories, operated by the Association of Universities for Research in Astronomy, Inc., under contract with the National Science Foundation.
[b] NOAO is operated by the Association of Universities for Research in Astronomy, Inc., under contract with the National Science Foundation.

 0004-6256/89/010107-24$00.90

CCD U (UG2 + liquid $CuSO_4$) and "Mould" interference B and V. Each CCD frame consisted of 316×500 pixels (after trimming), at a scale of 0.49 arcsec/pixel providing a field 2.5×4.0 arcmin in size, with the long axis oriented E–W. Flatfield exposures were made each afternoon of the "punto blanco" (white spot), illuminated by three projection lamps with color-balance filters. We found that while these flatfield exposures were adequate for removing the pixel-to-pixel sensitivity variations, exposures of twilight were needed to adequately remove large scale gradients, particularly in the U and B filters. Twilight sky was observed as much opposite the recently set Sun as possible to reduce any possible polarization effects. At the time, we attributed the differences in the flatfield calibration between twilight and the dome flats to be due to the color difference between them: the color-balanced dome flats had a color of $B - V \approx 0.5$, while the twilight-sky color was more like $B - V \approx -0.5$. As the latter was closer in color to the colors of the stars we were primarily interested in, we were not surprised that the twilight skys did a better job on our (mostly blue) standards, which we observed at several positions in the chip. However, subsequently Alistair Walker (CTIO memorandum) has found that twilight skys observed on this telescope do a better job of flattening even for red stars.

The fact that we had observations of standard stars over nine photometric nights allowed us to investigate the transformation equations and aperture corrections (star profiles) in a more detailed way than would have been possible during a shorter photometric run. Although the data discussed here for LH 117 and 118 were all obtained on a single night, the use of standards from the other nights has allowed us to make a better determination of the color terms in the transformation equations and the instrumental zero points. As we will use these transformations for other fields, and as we suspect this information will be useful to other observers, we will discuss our standard solution in some detail in the next section.

1) Standard star solutions

Standards from the list of Landolt (1983) were observed every night. We intentionally limited ourselves to fairly blue standards, as our experience had shown that adequate transformations could be achieved only over a fairly limited range in color, particularly at U, where the response of the CCD is dying. Typically, observations of five to seven standards were made seven to ten times per night in each filter. Care was taken to bracket the airmass range over which we observed the LMC and SMC. Table I lists the standards used in this project.

Integration times for the standards ranged between 1 and 150 s. During the year following our run, the camera interface was rebuilt, and it was subsequently found by Walker (1988) that the effective shutter time was about 30 ms longer than the specified length. We have looked for this effect in our data, by comparing standards of similar colors observed with short exposure times and long exposure times, and have derived a correction of 25 ms, in accord with Walker's value.

In obtaining digital aperture photometry of the standard stars on the CCD frames, a decision had to be made as to whether to do a curve-of-growth analysis and attempt to correct a finite aperture to one of infinite radius, or to simply adopt some radius to which all photometry would be referred—and if so, what radius? The latter method is what in practice is done in doing standard photoelectric aperture photometry, with good results. On the one hand, one would like to use as large an aperture as possible to include as much of the light as one can, but as apertures of larger and larger radii are used there is increased contribution from sky, as well as bad pixels, "cosmic rays" (radiation events), and so on (cf. Stetson 1987). At small radii, however, where the signal-to-noise is the best, the effect of seeing and telescope focus dominate the star profile, leading to inconsistent results from one frame to another. Although the seeing was typically 1.3–1.7 arcsec (2.5–3.5 pixels), increasing the digital aperture size from a diameter of 18 arcsec to one of 20 arcsec resulted in an additional 1%–2% increase in light for a well-exposed star, and this increase continues for larger apertures until masked by the photometric errors.

However, the fact that photoelectric photometry through a fixed aperture in fact does work suggests that there is some radius beyond which the same fraction of the light is excluded, despite variations in the seeing. Van de Hulst (1952), and more recently King (1971) and Kormendy (1973), discuss the profiles of stars obtained on photographic plates, and note that profiles of bright stars are detectable at radii of *arcminutes*, at brightness levels far greater than expected simply from the diffraction profile. Kormendy (1973) makes a convincing case that these faint wings are due to scattering off mirror dust and irregularities, and it is perhaps unsurprising then that we see faint additional light in our largest apertures. These faint wings of the point-spread function (PSF) should simply scale with the core of

TABLE I. Standard stars observed and residuals.

Star	V	$B-V$	$U-B$	Residuals									Comment
				$<U>$	σ_U	n	$<B>$	σ_B	n	$<V>$	σ_V	n	
GD246	13.090	−0.317	−1.188	−0.009	0.017	8	0.008	0.017	9	0.011	0.012	10	
GD71	13.027	−0.255	−1.099	0.003	0.019	13	0.008	0.012	12	0.005	0.015	13	
Feige 11	12.061	−0.236	−0.978	0.011	0.015	15	−0.004	0.012	15	0.000	0.009	15	
Feige 24	12.409	−0.199	−1.172	−0.018	0.016	11	0.010	0.011	11	−0.007	0.012	9	
99–438	9.399	−0.155	−0.719	0.003	0.008	8	−0.007	0.015	6	−0.002	0.007	7	
BD-2 524	10.307	−0.104	−0.641	0.006	0.019	6	−0.012	0.015	6	0.010	0.013	6	
BD-11 162	11.190	−0.081	−1.138	0.021	0.005	4	0.010	0.014	5	−0.002	0.011	6	
98-653	9.538	−0.004	−0.097	−0.011	0.014	6	−0.005	0.013	9	−0.012	0.011	11	
93-326	9.569	+0.454	−0.039	—	—	0	0.016	0.016	2	0.004	0.015	3	
96-36	10.589	+0.250	+0.111	—	—	0	−0.015	0.019	12	−0.004	0.013	12	Too red for U solution.
115-271	9.695	+0.619	+0.099	—	—	0	—	—	0	—	—	0	Too red for U or B.

the PSF, which is confirmed for the photographic case by Kormendy's careful photometry. Therefore, selecting a fixed-size aperture should merely exclude the same fraction of light, and the choice will not matter as long as the aperture is large enough to be insensitive to seeing, guiding, and focus variations.

We were therefore driven to ask at what radius this occurs on our frames. Since we had $\approx$300 standard-star observations at our disposal, we could investigate this in some detail. We used a series of concentric apertures and looked at the differences between various combinations of apertures. We found that the aperture correction from a radius of 3 pixels to infinity could vary anywhere from 0.25 to 1.25 mag, depending upon the seeing. However, essentially all of the *variations* in these aperture corrections occur at radii equal to or smaller than 8 pixels (diameter 8 arcsec). This is about the smallest size aperture that one would typically use for photometric aperture photometry and, given that one does not have the additional centering error that one does with photelectric work, is a reasonable value. At 10 pixels radius (10 arcsec diam) there was still a significant amount of light excluded compared to larger apertures, but little variation in this fraction from frame to frame. (The amount of light excluded by the 10-pixel-radius aperture compared to one of 15 pixels was 0.024 mag in the V filter, 0.025 mag in the B filter, and 0.031 mag in the U filter, with scatter at the few millimagnitudes level.) We adopted a 15 pixel radius (15 arcsec diam) aperture for measuring our standards.

Transformation equations of the form

$$u = U + A0 + A1\times(U-B) + A2\times X,$$
$$b = B + B0 + B1\times(B-V) + B2\times X,$$
$$v = V + C0 + C1\times(B-V) + C2\times X$$

were used, where UBV are the standard magnitudes, ubv are the instrumental magnitudes measured through the 15-pixel-radius digital aperture, X is the airmass, and $A0,\ldots C2$ are coefficients that must be determined from the standard-star observations. In solving these equations, we used Peter Stetson's CCDCAL package, which weights each observation inversely by the square of its uncertainty. The uncertainty is the quadrature sum of the observational uncertainty (estimated from the read-noise properties of the chip and photon statistics) and the quoted uncertainty of the standard magnitude listed by Landolt (1983).

The color terms ($A1$,$B1$,$C1$) are not expected to change during the course of the run, as these color terms are simply due to the mismatch between our instrumental bandpasses and the standard Johnson UBV bandpasses. Our instrumental bandpasses are the convolution of the mirror reflectivities, the filter transmissions, and the chip response. Of these, only the reflectivity of the mirrors is likely to change with time, and then we may expect significant changes only after several months, not during the course of a single run. We expect the color terms at U and B to be significant: at U the chip response is falling off very rapidly towards shorter wavelengths, and the Mould B filter is known to have an effective wavelength that is shifted several hundred Ångstroms redwards of the standard B bandpass, usually leading to a large color term, ≈ -0.2, even with chips with good UV and blue sensitivities (Massey, Jacoby, and Neese 1987). Similarly, the zero points ($A0$,$B0$,$C0$) are a measure of how stable the instrument is during the course of the run, and one would hope that this is better than 1%.

We therefore first solved these equations night by night, allowing each of the three terms to vary in each equation. As expected, the color terms and zero points were found to be very similar night to night. Accordingly, we reran the solutions after first fixing the color terms to the average value during the run. This did not increase the night-to-night scatter, showing that there was no mathematical justification for including the additional degree of freedom, and that the zero points were constant to within the observational uncertainties. Finally, we solved the equations with the zero points fixed to the average value. Again, we found no increase in the nightly scatter. This procedure should result in the best determination of the extinction and transformation constants. (An attempt to fix the extinction to an average value and allow, say, the zero points to vary increased the nightly scatter greatly, in accord with our expectations.)

The zero points and color terms adopted were as follows:

$$u = U + 4.949 - 0.354\times(U-B) + A2\times X,$$
$$b = B + 2.313 - 0.222\times(B-V) + B2\times X,$$
$$v = V + 2.495 + 0.007\times(B-V) + C2\times X.$$

The size of the zero points indicates the relative sensitivity of the system (primarily the chip, as the filters all have similar bandwidths and transmissions). Table II shows the change of extinction over the course of the run, and the amount of "additional nightly scatter," i.e., what errors are present over and above what we would expect given the estimated errors on the instrumental and standard magnitudes. We see that the average scatter of the standard solutions is approximately 0.015 mag for these "all sky" solutions. We expect then, regardless of other errors, that our colors are unlikely to be determined in an absolute sense to better than 0.020 mag.

We list in Table I the average residuals of each standard star ($\langle U\rangle$,$\langle B\rangle$,$\langle V\rangle$), the standard deviations of the residuals (σ), and the number of observations of each star in each

TABLE II. Extinction terms and additional nightly scatter.

	22/11/85	23/11/85	24/11/85	25/11/85	26/11/85	27/11/85	28/11/85	29/11/85	02/12/85
$U(A2)$	0.438	0.413	0.437	0.440	0.453	0.503	0.504	0.462	0.439
$B(B2)$	0.229	0.235	0.234	0.245	0.244	0.277	0.275	0.250	0.230
$V(C2)$	0.139	0.148	0.142	0.152	0.147	0.180	0.174	0.158	0.135
σ_U	0.012	0.008	0.024	0.020	0.024	0.016	0.021	0.020	0.020
σ_B	0.019	0.015	0.019	0.016	0.006	0.037	0.014	0.020	0.018
σ_V	0.008	0.009	0.014	0.015	0.020	0.014	0.010	0.016	0.012

filter (n). Significant deviations from a linear color term occur in the transformation of U near $U-B\approx 0$. Similarly, a linear color term at B was adequate only for $B-V<0.5$. We attempted to use higher-order terms in the color equations (including standard stars redder than those listed), and while it was possible to obtain transformations that performed better over a wider range of colors, we found that the residuals for the bluest stars were always increased. Since we are primarily interested in the photometry of stars whose colors are well fit by the linear solution described above, we retained this solution and accept that stars redder than the limits given will have poorer photometry.

2) The program fields

The *UBV* observations of LH 117 and LH 118 were all made on the night of (UT) 25 November 1985 between an airmass of 1.30 and 1.35. In order to cover these two associations, exposures were made of five fields: two fields for LH 117 (designated "N" and "S" for north and south in the following), and three on LH 118 (designated north, south, and "extra" ("X")). Figure 1 [Plate 9] shows the location of the fields, along with the outlines of the associations taken from Lucke's thesis (Lucke 1972). The identification of bright blue stars from Sanduleak (1969) are also shown. Table III gives the exposure information for each field. Both short and long exposures were employed to extend the range of magnitudes usefully studied. The "extra" field on LH 118 were intended primarily to obtain photometry of Sk $-70°117$ and Sk $-70°118$ and no long exposure was made at that position.

The frames were analyzed in Tucson on a VMS VAX 8600 and VAX 750 using DAOPHOT (Stetson 1987). Isolated stars were used to define the PSF on a frame, and the resulting profile fit simultaneously to all the stars in a region. In reducing the frames, care was taken to compare the identification of stars on the U, B, and V frames of the short exposures to make sure of consistent identification of stars, particularly in the most crowded regions. The long exposures were treated similarly, and as a final step the identifications on the short and long exposures were compared.

The zero point for the instrumental magnitudes was defined for each frame by an aperture of 3 pixels radius, and it was necessary to determine the correction for each frame from this small radius to the 15 pixel radius with which the standards were measured. It is our experience that it is this aperture correction that is the most uncertain in the photometry of stars in relatively crowded regions, but the comparison of stars in common between the short and long exposures, and in the overlap regions of the frames, was usually reassuring. As the shorter exposures had only a few stars with good photon statistics to use for the determination of aperture corrections—sometimes only one—we believe that it is the shorter frames (and hence brighter stars) that may have the most absolute errors in their photometry.

TABLE III. Fields observed.

Field	α_{1950}	δ_{1950}	Exposure Time (sec)		
			U	B	V
LH117N	05 49 26.0	-70 03 46	1000,80	300,20	300,20
LH117S	05 49 20.0	-70 05 59	1000,80	300,20	300,20
LH118N	05 50 06.3	-70 05 25	1000,80	300,20	300,20
LH118S	05 50 06.4	-70 07 15	1000,80	300,20	300,20
LH118X	05 50 03.2	-70 09 01	80	20	20

The transformation equations given above were applied to stars that were identified in all three filters, using the instrumental colors as a starting point and iterating. As a first step, the short and long exposures of each field were treated separately. However, since the U exposure times were chosen (see Table III) so that a blue star would have similar counts on all three filters for either the short or long exposures, it was necessary also to combine the photometry of the long U exposure with the short B and V exposures of each field in order to pull out the photometry of any bright red stars that were saturated on the long B and V exposures but invisible on the short U exposure and hence would have been missed. This resulted in the addition of three stars to the final photometry list for the five regions.

The final photometry is given in Table IV for LH 117 and in Table V for LH 118. In many cases there were multiple observations of the same star (from short and long exposures, or stars in regions of overlap within LH 117 or LH 118). For these stars we have averaged the photometry, weighting each observation inversely by the square of its error. The stars are identified in Figs. 2 and 3 [Plates 10 and 11] for LH 117, and in Figs. 4–6 [Plates 12–14] for LH 118. The stars within each association are numbered from north to south (from low x to high x on our frames). We have shown the identification numbers in the figures for the least crowded of the brighter stars, and the identification of other stars can be inferred from their x and y values within each frame. All stars for which we give photometry are marked with dots.

Figure 7 shows the formal errors as a function of magnitude for the photometry of stars in Table IV (LH 117), and Fig. 8 shows the errors for the photometry of stars in Table V (LH 118). The larger errors in the latter near 17th magnitude are due to the fact that only the short exposures were available for the "extra" field LH 118X. The errors in Figs. 7 and 8 are those estimated by DAOPHOT not only on the basis of the chip characteristics and exposure level, but also on how well the point-spread function fit the star profile. Thus, at a given magnitude there will be some scatter. We give in Table VI the "typical" error as a function of magnitude, judged by eye from Figs. 7 and 8, and excluding the stars on LH 118X. In Tables IV and V we have marked by a colon any entry whose error is worse than twice this typical error at a given magnitude and by two colons any entry whose error is estimated to be 3σ or greater. In addition, colons are added for stars whose colors lay outside the limits well fit by the linear transformation equations adopted, and for stars whose "chi values" (a measure of how well the point-spread-function fit) exceeded 2.0.

The actual photometric errors are hard to evaluate, as there are few external checks available. One "internal" check comes about as two stars occur on both our LH 117 and LH 118 tables. We see in Table VII that in fact our measurements of the brighter of these stars (LH 117-103 = LH 118-012) differ badly. However, as can be seen in Figs. 2 and 4, this star is just barely on the edge of the LH 117 frames, but is well located on the LH 118 frames (see also Fig. 1). Its photometry is flagged in Table IV as uncertain due to a poor point-spread-function fit on the B frame, consistent with the nature of the differences seen in Table VII. For the fainter star (LH 117-090 = LH 118-004) the agreement is good.

1989AJ.....97..107M

TABLE IV. Photometry of LH 117.

Star	X	Y	V	U-B	B-V	Star	X	Y	V	U-B	B-V	Star	X	Y	V	U-B	B-V
1	21.0	165.0	17.50	-0.57	-0.09	51	183.4	300.7	16.10	-0.92::	-0.05::	101	241.7	351.7	17.17	-0.73	-0.14
2	33.7	5.3	18.11	-0.26:	-0.06	52	183.9	134.1	18.17	-0.92	0.19	102	244.5	244.7	19.06	-0.23:	0.07
3	36.0	295.9	17.41	0.20::	0.84:	53	184.7	275.8	16.78	-0.30:	0.05	103	244.3	4.5	13.50	-0.87::	-0.12::
4	38.4	146.4	18.59	-0.22:	-0.05	54	185.1	126.1	16.54	-0.59	-0.10	104	245.7	134.9	17.88	-0.52	-0.01
5	38.9	333.3	18.56	-0.32:	-0.03	55	185.6	162.3	16.04	-0.91::	-0.14::	105	247.6	140.5	18.66	-0.47	-0.07
6	56.7	163.9	17.09	-0.85	-0.12	56	188.7	171.0	18.95	-0.56	-0.24	106	249.3	268.6	14.52	1.12::	0.85:
7	64.6	124.6	18.70	-0.02:	-0.07	57	188.1	116.5	17.68	-0.90	-0.10	107	268.8	204.9	17.98	0.02::	0.43
8	72.7	315.1	16.90	0.26::	0.14	58	190.7	359.8	18.80	0.61::	0.00	108	270.2	255.3	15.77	-0.88	-0.19
9	80.9	357.5	18.91	-0.20:	0.06	59	190.7	109.6	18.04	0.13::	0.44	109	270.6	157.5	18.09	-0.62	-0.12
10	83.6	65.5	18.27	-0.42	-0.07	60	191.5	117.2	17.41	-0.70	-0.07	110	272.9	277.6	16.72	-0.82	-0.16
11	84.1	242.5	18.51	0.05::	-0.06	61	191.9	291.3	17.36::	-0.97:	0.31::	111	272.5	317.8	17.40::	-0.58::	-0.18::
12	86.5	298.1	17.54	-0.59	-0.11	62	191.3	295.4	14.73	-0.84	-0.12	112	272.8	250.6	17.80:	0.87::	0.96:
13	90.2	339.8	19.08	-0.20:	-0.04	63	192.4	170.2	18.89:	-0.53	0.23	113	275.2	305.5	17.60	-0.71	-0.04
14	105.2	263.8	14.69	-0.88	-0.05	64	194.9	414.8	12.67	2.23::	1.71::	114	276.6	274.1	18.89	-1.05	0.14
15	105.3	232.3	16.60	-0.78	-0.04	65	195.7	442.7	18.63	-0.19:	0.16	115	277.5	175.3	17.16	-0.65	-0.14
16	106.1	178.0	12.09	-0.70	0.08	66	196.8	152.4	16.64	-0.88::	-0.14::	116	282.8	283.4	18.57	-0.49	-0.11
17	110.9	368.7	18.61	-0.25:	-0.04	67	200.8	152.8	15.50	-0.88	-0.15	117	283.7	137.6	15.76	0.85::	0.81:
18	115.3	244.4	17.16	-0.72	0.05	68	201.3	158.7	17.95	-0.60	0.58	118	284.7	316.6	12.23	-0.92	-0.11
19	120.8	157.9	15.25	-0.79	-0.12	69	201.4	294.6	18.07	-0.95	0.01	119	284.6	329.2	16.10	-0.88::	-0.12::
20	127.6	278.7	16.84	-0.78	-0.13	70	202.0	314.6	18.47	-0.63	-0.05	120	287.4	249.8	16.83	-0.84	-0.13
21	127.4	356.4	18.08	-0.13:	-0.01	71	203.7	129.3	16.87	-0.62	-0.16	121	290.7	370.9	17.60::	-0.40::	0.19::
22	128.6	329.1	19.34	-0.59	0.12	72	203.2	344.2	17.54	-0.63	-0.01	122	292.1	330.2	16.53	-0.12:	0.56
23	135.6	434.6	16.09	-0.75	-0.13	73	205.4	308.3	15.70	-0.81:	-0.14:	123	295.0	264.1	17.42	-0.82	-0.08
24	140.1	248.4	18.41	-0.15:	0.10	74	206.0	316.7	18.05	-0.30:	-0.06	124	295.0	289.1	18.86	-0.98:	0.20:
25	147.5	153.8	18.34	1.42::	0.38	75	206.9	192.0	18.53	-0.64	0.20	125	296.7	174.7	17.64	-0.74	-0.11
26	153.1	447.0	18.38	-0.08:	0.08	76	206.9	196.1	18.17	-0.86	0.16	126	31.3	25.0	17.84	-0.38:	0.00
27	155.7	84.0	17.70	-0.65	-0.05	77	207.9	274.6	18.20	-0.72	0.05	127	34.3	219.7	16.68	-0.68	-0.14
28	156.8	78.8	17.77	-0.55	-0.06	78	207.2	442.0	17.02	-0.51	0.02	128	34.9	147.9	16.22	-0.82	-0.12
29	156.5	458.8	16.53	-0.84	-0.15	79	207.9	428.7	18.40	-0.23:	0.56	129	36.5	223.2	17.58::	-0.76:	0.05::
30	159.5	88.9	16.52	-0.86	-0.16	80	208.1	302.9	15.66	-0.80::	-0.07::	130	36.2	254.0	17.34	-0.73	-0.02
31	162.0	118.0	16.01	-0.88	-0.18	81	209.9	67.0	18.56	-0.64	-0.22	131	39.4	176.4	15.61	-0.95	-0.17
32	163.8	92.8	18.70	-1.03	-0.04	82	212.7	285.6	16.28	-0.85	-0.12	132	39.8	219.2	17.36:	-0.71	0.00
33	164.4	63.4	16.58	0.36::	0.33	83	212.4	259.3	17.39	-0.57	-0.01	133	40.3	324.6	17.36	-0.62	-0.04
34	164.6	81.0	16.93	-0.79	-0.16	84	213.3	152.1	17.53	-0.68	-0.12	134	40.8	270.2	16.77	-0.80	-0.09
35	165.5	226.9	18.34	-0.54	0.05	85	214.2	111.0	19.12	-0.44	0.16	135	40.8	212.1	16.23	-0.87:	-0.12:
36	170.7	334.9	18.44	-0.48	-0.07	86	217.3	429.8	18.66	-0.14:	0.34	136	45.5	217.3	16.72	-0.39:	-0.20::
37	171.0	264.9	17.74	-0.66	-0.14	87	221.2	313.5	18.17	-0.55	0.04	137	46.2	226.8	15.83	-0.86	-0.06
38	173.3	135.6	18.00:	-0.27:	0.01:	88	223.8	106.3	17.87	-0.05:	0.13	138	49.5	222.5	17.76:	-0.50::	-0.01::
39	175.5	135.7	17.44::	-0.43:	-0.22:	89	223.5	252.1	18.46	-0.40:	0.16	139	51.5	229.2	18.74:	-1.00:	0.16
40	176.1	68.1	16.26	-0.77	-0.19	90	223.9	72.1	15.00	-0.74	-0.14	140	52.3	216.5	13.52	-0.98	-0.11
41	177.5	400.8	18.84	-0.37:	0.22	91	225.8	321.6	16.92	-0.81	-0.01	141	53.4	293.0	18.07	-0.35:	-0.06
42	178.0	186.5	18.35	-0.49	0.16	92	226.0	419.8	16.89	-0.80	0.03	142	54.6	157.3	18.30	-0.49	-0.01
43	178.1	113.0	14.08	-0.99	-0.18	93	230.9	251.5	17.79	-0.65	0.01	143	54.8	218.7	16.47::	-0.87::	0.02::
44	178.6	251.7	18.07	-0.50	0.11	94	231.4	325.2	19.15	1.29::	0.22	144	56.0	444.1	15.23	-0.80::	0.00::
45	179.5	110.3	17.47::	-1.16::	-0.40::	95	231.5	119.7	18.77	-0.23:	-0.09	145	56.5	233.2	17.04	-0.71	-0.03
46	180.9	108.1	17.44:	-0.36::	0.06::	96	234.6	42.8	18.51	-0.52	-0.13	146	58.0	259.0	14.75	-0.87:	0.02:
47	180.1	197.2	19.44	-1.34	0.17	97	234.9	272.1	16.46	-0.73	-0.14	147	60.0	210.7	17.80::	-0.71	0.23::
48	181.2	475.3	18.51	-0.03:	0.12	98	236.7	232.6	14.94	-0.88	0.02	148	61.0	301.4	16.39	-0.75	-0.08
49	181.6	160.6	16.98	-0.89::	-0.11::	99	239.5	222.6	16.37	-0.86	-0.10	149	70.8	225.4	19.28	-0.61	-0.19
50	182.2	360.9	16.68	-0.74	-0.17	100	241.4	313.1	18.06	-0.56	-0.08	150	71.1	220.0	18.16	-0.32:	-0.14

TABLE IV. (continued)

Star	X	Y	V	U-B	B-V	Star	X	Y	V	U-B	B-V	Star	X	Y	V	U-B	B-V
151	72.7	207.9	16.71	-0.80	-0.05	181	131.8	216.1	17.97	0.56::	0.67:	211	194.1	319.2	18.31	-0.40:	-0.03
152	75.3	336.3	14.03	-0.92	-0.09	182	133.3	82.0	18.67	-0.36:	0.31	212	198.4	424.0	14.94	0.44::	0.67:
153	82.0	208.5	18.17	-0.29:	-0.12	183	134.9	196.8	15.08	-0.96	-0.15	213	206.5	320.1	16.83	-0.60	-0.08
154	83.1	254.7	15.24	1.52::	1.08::	184	136.0	312.8	15.97	-0.81:	-0.04:	214	207.1	258.5	13.29	-1.09	-0.19
155	86.3	214.1	17.18	-0.52	0.01	185	138.6	288.9	17.65	-0.52	-0.09	215	208.0	69.2	18.01	1.06::	0.75:
156	86.6	231.1	18.14	-0.63	-0.08	186	138.2	149.0	16.15	-0.78::	-0.05::	216	215.2	335.8	17.44	-0.49	0.33
157	89.6	296.9	17.10	-0.75	-0.06	187	138.1	358.9	14.61	-0.95:	-0.14:	217	220.5	437.7	15.71	1.96::	1.05::
158	89.0	464.9	16.71	-0.59	0.09	188	139.2	143.9	16.13	-0.91::	-0.11::	218	220.6	102.2	17.74	-0.42	-0.02
159	90.3	217.9	16.58	-0.84::	-0.15::	189	140.4	171.0	18.12	-0.13:	0.05	219	221.8	69.3	17.81	-0.62	-0.01
160	90.1	267.6	17.97	-0.52	-0.06	190	147.3	350.5	18.40	-0.91	0.00	220	230.0	344.9	16.64	-0.67	-0.05
161	90.4	227.6	17.70	-0.59	-0.07	191	148.2	235.3	15.93	-0.76:	-0.11:	221	230.3	356.1	18.42	1.10::	0.05
162	91.3	271.3	18.04	-0.59	-0.05	192	152.6	194.7	18.02	-0.39:	0.19	222	256.0	292.8	17.76	-0.66	-0.11
163	90.8	323.3	17.94	-0.63	-0.03	193	152.8	188.7	17.37	-0.40:	0.04	223	257.0	371.5	16.11::	-0.82::	0.20::
164	96.6	270.5	18.65	0.05::	0.11	194	154.7	185.5	17.29	-0.55	0.05	224	283.5	241.2	15.94	-0.84	-0.13
165	100.0	74.5	16.48	-0.87::	-0.12::	195	162.5	190.2	18.03	-0.41	0.83:	225	284.0	369.4	18.43	-1.02	0.11
166	104.2	167.8	18.27::	-0.44::	-0.18:	196	166.8	301.1	18.59	-0.44	-0.06	226	312.2	369.7	16.94	0.62::	0.94:
167	111.8	136.2	18.22	-0.59	-0.15	197	167.8	308.3	15.10	-0.89	-0.15						
168	112.6	255.3	15.67	-0.94::	-0.17::	198	169.6	241.2	15.47	-0.89	-0.14						
169	113.2	237.5	15.10	0.91::	0.89:	199	169.6	186.4	18.51	-0.07:	0.05						
170	114.8	221.8	16.58	-0.69:	-0.06	200	170.9	212.0	17.00	-0.71	-0.08						
171	116.0	261.4	18.46	-0.47	-0.10	201	176.6	340.8	19.22	-0.69	-0.08						
172	115.9	226.8	18.20	0.00:	0.08	202	180.7	307.6	17.91	-0.60	-0.05						
173	119.8	206.8	18.91	-0.32:	-0.09	203	183.5	322.9	16.93	-0.69::	-0.11::						
174	121.4	218.5	16.27	-0.72::	-0.11::	204	182.8	213.8	17.82	-0.58	-0.12						
175	121.9	260.8	16.68	-0.62::	-0.08::	205	185.9	318.3	19.21	-0.18:	-0.41						
176	122.8	203.2	17.60	-0.61	-0.12	206	187.6	328.2	15.06	-0.93	-0.18						
177	124.1	239.7	18.30	-0.36:	0.00	207	188.8	317.3	17.95	-0.65	-0.10						
178	125.8	395.6	18.24	-0.33:	-0.04	208	188.7	495.0	18.34	0.20::	0.38						
179	127.4	170.3	16.40	-0.65::	-0.04::	209	190.3	354.3	17.57	-0.29:	0.04						
180	128.7	367.9	18.24	-0.50	0.08	210	192.9	339.4	17.85	-0.42	-0.03						

1989AJ.....97..107M

TABLE V. Photometry of LH 118.

Star	X	Y	V	U-B	B-V	Star	X	Y	V	U-B	B-V	Star	X	Y	V	U-B	B-V
1	5.1	306.4	18.19	-0.28:	0.03	51	120.3	109.5	17.98	-0.51	0.08	101	201.4	473.9	15.92	0.37::	0.31::
2	8.7	340.8	16.31	-0.70:	-0.06:	52	120.4	1.8	16.99	-0.65	0.02	102	201.6	40.9	18.18	-0.21:	0.08
3	13.4	437.3	19.17	0.58::	0.09	53	121.4	229.4	18.46	-0.11:	0.43	103	203.8	359.3	19.00	-0.41	0.44
4	14.5	488.1	15.00	-0.73:	-0.07:	54	123.8	380.3	18.99	-0.36:	-0.10	104	205.4	417.1	17.80	0.07::	1.05::
5	16.1	331.4	17.02	-0.68::	-0.05::	55	126.8	423.7	19.49	-0.46	-0.25	105	207.1	203.8	15.00	-0.91::	-0.13::
6	16.7	267.8	17.86	0.70::	0.81:	56	127.0	216.3	16.19	-0.76::	-0.10::	106	207.7	62.1	19.48	-0.63	-0.04
7	25.0	458.9	18.50	-0.68	0.02	57	129.3	259.2	18.76	-0.05:	-0.02	107	209.9	29.0	18.17	0.05::	0.02
8	26.0	213.6	18.67	0.22::	0.12	58	132.2	345.9	18.16	-0.65	-0.06	108	211.4	184.0	17.98	-0.26:	0.20
9	28.3	164.6	17.36	-0.76	-0.12	59	133.0	403.6	18.93	-0.13:	0.22	109	211.8	6.7	18.94	-0.22:	0.19
10	30.5	478.0	19.20	-0.84	0.20	60	135.4	87.0	17.72	-0.01:	0.52	110	212.1	262.3	15.83	-0.92::	-0.15::
11	31.6	358.8	18.60	-0.15:	-0.02	61	138.2	35.5	16.59	0.64::	0.81:	111	215.5	137.0	19.01	-0.32:	-0.06
12	34.8	420.5	13.53	-1.00	-0.08	62	142.3	228.3	17.25	-0.49	0.00	112	216.0	177.9	18.35	-0.22:	0.35
13	35.2	242.2	18.27	-0.44	0.03	63	142.4	364.5	18.20	-0.75	0.05	113	219.0	104.7	18.26	-0.15:	0.09
14	36.9	235.4	19.50	-0.56	0.05	64	144.4	302.7	17.27	-0.65	-0.09	114	219.6	96.5	19.07	-0.78	0.77:
15	36.9	148.6	18.74	-0.07:	0.11	65	145.0	218.6	18.49	-0.40:	0.24	115	221.1	12.1	18.38	-0.03:	0.01
16	39.0	368.4	17.35	-0.70	-0.04	66	147.0	379.3	16.57	1.42::	1.16::	116	224.2	141.5	14.90	-0.87::	-0.14::
17	40.0	398.8	18.31:	-1.28	0.80:	67	149.3	54.1	19.09	-0.33:	0.18	117	226.1	151.2	18.52	-0.27:	0.07
18	41.7	349.5	17.93	-0.11:	0.21	68	152.5	12.4	18.43	-0.15:	0.02	118	228.5	40.5	15.71	1.98::	1.40::
19	43.3	414.0	17.75::	0.42::	-0.58::	69	153.1	49.1	18.01	-0.37:	-0.03	119	233.1	84.4	18.98	0.26::	0.09
20	43.8	36.8	15.84	-0.85::	-0.14::	70	153.4	26.9	18.40	-0.08:	0.15	120	234.8	97.1	18.78	0.16::	0.30
21	52.9	434.3	19.57	-0.23:	-0.33	71	154.4	459.8	12.22	0.29::	0.60	121	236.6	225.9	17.21	-0.63::	-0.10::
22	55.8	274.4	18.85	-0.34:	0.10	72	161.3	298.2	15.45	0.15::	0.64:	122	241.4	315.0	17.93	-0.40	-0.03
23	58.3	49.8	19.49	-0.70	0.31	73	162.6	343.5	19.20	-0.16:	-0.34	123	242.4	180.7	18.34	0.03::	0.51
24	58.8	129.3	16.36	-0.66::	-0.07::	74	163.0	223.1	18.34	-0.01:	-0.23	124	242.7	384.3	18.35	-0.65	0.04
25	59.6	351.1	18.42	-0.38:	-0.04	75	163.0	215.1	17.49::	-0.59:	-0.20::	125	250.8	10.3	19.39	-0.66	-0.11
26	62.0	429.9	18.76	-0.46	0.50	76	163.9	228.8	16.44	-0.83::	-0.14::	126	252.2	349.7	19.34	-0.19:	-0.04
27	75.7	146.8	18.21	-0.43	-0.03	77	164.5	254.3	18.21	-0.17:	0.32	127	254.3	116.8	18.49	-0.10:	0.07
28	76.5	43.2	18.90::	-1.46	1.18::	78	165.1	215.2	15.82:	-0.88	-0.09:	128	255.1	73.4	17.40	0.97::	1.16::
29	78.7	31.1	18.75	-0.47	0.10	79	168.4	219.8	16.12	-0.75::	-0.12::	129	255.2	157.5	18.82	-0.63	-0.17
30	79.6	133.5	18.97	0.67::	0.04	80	169.4	234.4	18.32	-1.15	0.04	130	256.9	496.7	17.16	1.23::	1.24::
31	82.9	369.3	19.23	-0.35:	0.16	81	171.0	236.5	17.56	-0.16:	0.02	131	257.5	198.7	19.01	-0.43	-0.05
32	84.4	99.3	18.59	0.36::	0.19	82	175.4	216.9	16.85	-0.87::	-0.11::	132	257.8	8.7	19.22	-0.58	0.25
33	84.8	68.5	18.47	-0.26:	-0.10	83	175.9	313.2	17.46	0.00::	0.15	133	261.7	140.3	17.78	-0.28:	0.04
34	87.8	191.7	15.77	1.74::	1.14::	84	179.2	8.0	19.47	-0.86	0.01	134	261.8	191.1	17.46	-0.65::	-0.12::
35	93.0	211.2	19.05	-0.67	0.13	85	179.6	31.6	18.71	-0.66	0.33	135	262.0	260.0	17.25	0.19::	0.62:
36	93.6	130.0	18.84	0.42::	-0.03	86	181.0	452.7	16.57	-0.82::	-0.08:	136	262.4	175.3	18.52	-0.23:	0.01
37	94.1	360.4	17.90	-0.35:	0.09	87	182.7	370.4	18.65	0.04::	0.13	137	264.7	134.5	18.72	0.42::	0.08
38	97.2	411.1	19.14	-0.91	0.39	88	183.8	231.5	17.45	-0.72	-0.03	138	265.7	164.0	13.94::	-0.89::	-0.18::
39	98.1	202.9	19.32	-0.52	0.25	89	186.9	158.1	18.47	-0.39:	-0.03	139	266.8	286.7	18.15	-0.47	-0.12
40	98.4	314.1	17.05	-0.81	-0.13	90	187.4	215.6	17.25	-0.59::	-0.07::	140	271.7	406.2	19.48	-0.14:	-0.14
41	99.1	296.0	16.99	-0.79	-0.14	91	187.7	55.0	16.55	-0.78::	-0.07::	141	272.4	217.4	17.03	-0.76:	-0.14
42	101.7	323.6	18.71	-0.76	-0.08	92	189.3	63.0	18.87	-0.75	-0.09	142	278.4	224.4	18.52	-0.27:	0.08
43	105.7	387.0	16.92	1.09::	1.18::	93	190.2	7.1	16.30	-0.87::	-0.13::	143	278.8	334.0	18.67	-0.25:	-0.05
44	106.9	6.6	19.24	-0.87	0.52	94	190.6	284.2	18.54	-0.70	-0.08	144	285.6	4.4	19.26	-0.50	0.37
45	110.3	46.8	18.82	-0.49	0.22	95	192.2	89.2	19.04	0.02::	0.27	145	285.8	310.3	18.17	0.22::	0.22
46	112.8	431.8	19.24	-0.41	-0.24	96	193.2	70.0	18.51	-0.34:	0.01	146	286.7	300.1	18.95	-0.62	0.01
47	114.1	290.0	19.44	-0.10:	-0.05	97	197.2	180.8	17.16	-0.74::	-0.15::	147	290.5	161.3	18.66	-0.12:	0.13
48	114.6	233.8	17.79	-0.60	-0.01	98	198.5	187.8	16.43	-0.89::	-0.11::	148	292.1	182.6	17.69	-0.69	-0.12
49	114.9	259.9	18.22	-0.50	0.04	99	198.7	468.2	17.32	-0.07:	0.10	149	293.7	227.8	19.21	0.05::	0.09
50	119.0	438.5	18.13	-0.50	-0.12	100	199.2	309.0	17.92	-0.04:	0.18	150	294.1	494.0	16.99	1.28::	1.08::

1989AJ.....97..107M

TABLE V. (continued)

Star	X	Y	V	U-B	B-V	Star	X	Y	V	U-B	B-V	Star	X	Y	V	U-B	B-V
151	294.8	115.5	18.01	0.09::	0.25	186	167.2	325.4	18.78	0.01::	-0.04	221	288.0	61.0	16.10	1.66::	1.08::
152	296.4	236.0	16.48	-0.79:	-0.15:	187	173.2	459.3	18.78	-0.05:	-0.06	222	288.8	139.5	15.85	-0.88::	-0.19::
153	79.9	247.7	18.46	-0.10:	0.00	188	176.4	164.8	19.39	0.22::	0.22	223	289.7	158.6	17.99::	-1.44	0.60::
154	80.9	215.9	15.82	-0.89::	-0.15::	189	177.2	385.5	19.07	-0.20:	-0.12	224	292.7	85.5	18.74	-0.01:	0.10
155	82.6	444.8	18.93	-0.42	0.30	190	183.4	440.3	17.46	-0.20:	0.03	225	295.3	305.9	12.69	2.69::	1.92::
156	91.6	419.2	16.55	0.06::	0.58	191	183.8	46.8	18.72	-0.15:	0.34	226	299.0	182.2	19.50	-0.16:	0.04
157	94.1	358.2	18.17::	-2.54	1.69::	192	185.1	345.2	19.26	-0.19:	-0.06	227	83.7	-12.0	17.74	-0.49	-0.08
158	94.7	18.7	18.95	0.01::	0.09	193	185.9	453.5	17.55	0.31::	0.26	228	84.8	219.2	18.65	-0.35:	-0.07
159	94.9	130.0	19.23	-0.58	-0.03	194	188.1	164.5	18.81	-0.26:	-0.01	229	85.5	88.2	17.08	-0.61::	-0.18::
160	99.6	135.6	19.14	-0.38:	-0.04	195	190.6	435.1	17.16	-0.62	-0.08	230	87.2	196.3	15.56	-0.85:	-0.21:
161	102.3	399.9	14.04	1.09::	0.87:	196	191.3	19.5	16.52	1.51::	1.37::	231	88.6	155.9	18.88	-0.04:	-0.13
162	102.6	386.5	15.85	1.41::	1.63::	197	192.4	92.3	15.39	-0.80	-0.16	232	109.0	260.4	17.05::	-0.29:	-0.07::
163	105.0	91.1	16.81	0.95::	0.88:	198	193.7	171.1	19.40	-0.10:	-0.02	233	112.7	111.3	16.68::	-0.40::	-0.19::
164	109.1	269.3	18.34	-0.44	-0.07	199	196.8	475.9	15.11	-0.77	-0.12	234	113.7	148.2	15.47:	-0.71	-0.21:
165	112.3	303.7	15.14	-0.93	-0.19	200	198.6	133.8	17.21	-0.66	-0.06	235	124.3	139.4	17.10::	-0.47::	-0.17::
166	117.4	290.3	18.84	0.05::	0.00	201	202.1	102.6	18.14	-0.17:	0.13	236	142.4	241.0	17.30::	-1.29::	0.19::
167	117.7	262.0	16.92	-0.66::	-0.14::	202	203.1	235.2	18.74	-0.58	0.01	237	146.9	167.7	15.87::	-0.66:	-0.14:
168	119.0	185.9	16.41	-0.77::	-0.14::	203	203.7	213.6	19.07	-0.95	0.01	238	154.1	169.0	17.02::	-2.12:	0.60::
169	119.3	202.9	15.84	-0.81:	-0.16:	204	214.1	157.4	16.33	-0.70::	-0.13::	239	157.3	188.6	13.23:	-0.82	-0.20
170	126.5	208.5	18.11	-0.50	-0.19	205	214.7	279.7	18.83	-0.47	-0.14	240	158.1	186.2	14.10::	-0.99::	-0.16::
171	128.4	107.0	17.42::	-1.25	0.38:	206	222.0	337.1	17.83	-0.39:	-0.19	241	159.0	161.8	13.35	-0.89	-0.23
172	130.1	162.0	17.66::	-0.90	0.27:	207	229.5	196.6	19.21	-0.19:	-0.02	242	165.5	265.6	17.50::	-0.50::	0.00::
173	139.1	174.1	17.64	-0.55	-0.11	208	231.8	280.6	18.10	-0.24:	-0.10	243	289.3	274.3	17.60::	-0.91::	-0.13::
174	142.9	200.8	16.51	0.85::	0.87:	209	232.8	453.8	16.61	-0.77::	-0.13::	244	307.9	120.0	13.72::	0.88::	0.71::
175	143.0	454.0	19.18	-0.28:	0.40	210	235.3	180.5	19.43	-0.70	0.37						
176	144.2	390.4	19.72	-0.42	-0.05	211	240.8	126.0	16.06	-0.85::	-0.18::						
177	147.9	153.8	18.25	0.20::	0.37	212	243.9	373.8	18.25	-0.20:	0.10						
178	149.9	480.9	17.46	0.43::	0.72:	213	245.8	216.2	18.74	-0.16:	0.36						
179	150.0	440.6	18.73	-0.42	0.15	214	255.5	491.0	16.79	1.61::	1.12::						
180	152.1	260.4	17.47	-0.51:	-0.05:	215	258.2	70.8	17.14	-0.69	-0.02						
181	159.2	272.4	18.11	-0.78	0.03	216	259.8	296.8	16.44	-0.85::	-0.13::						
182	162.4	400.3	13.88	-1.00	-0.19	217	269.9	150.3	17.52::	-1.09::	-0.20::						
183	164.1	235.5	16.73	1.68::	1.13::	218	272.0	99.9	18.85	-0.46	-0.20						
184	164.1	43.3	19.01	-0.20:	0.07	219	273.8	126.4	19.23	-0.62	-0.08						
185	166.9	246.8	18.71	-0.62	-0.08	220	274.6	249.5	18.65	0.10::	-0.03						

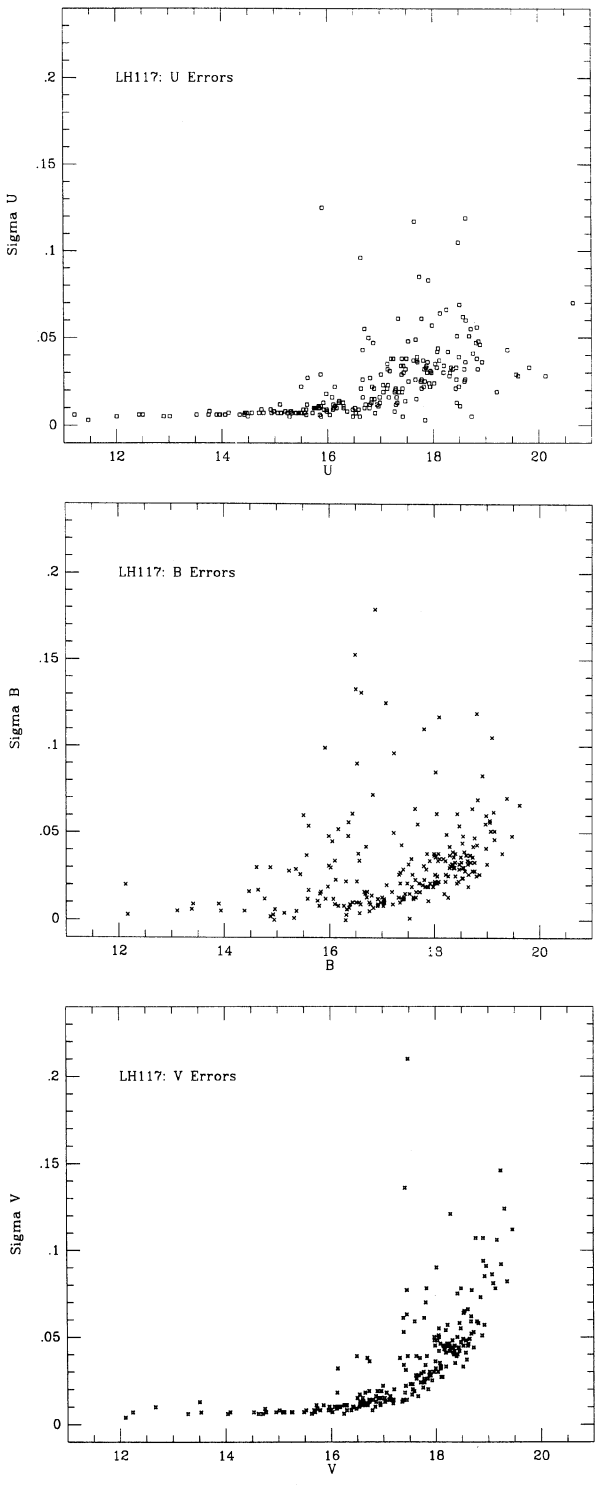

FIG. 7. Errors in the photometry of LH 117 as a function of magnitude.

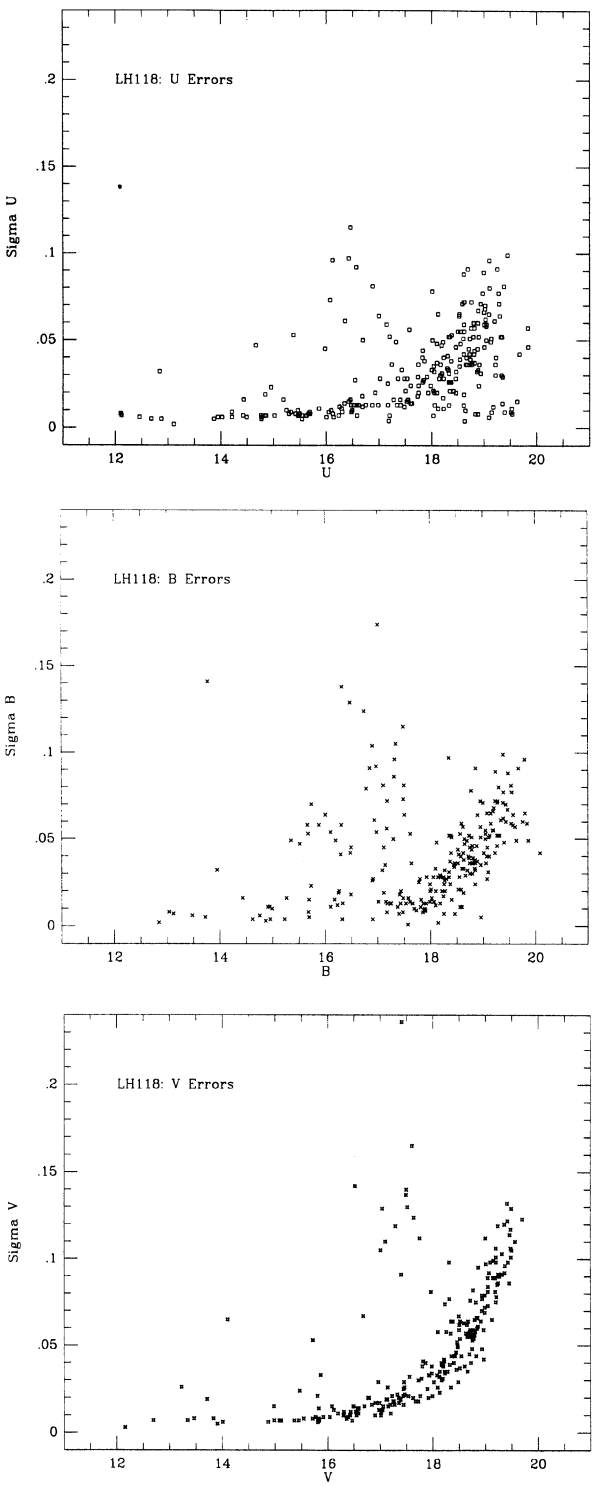

FIG. 8. Errors in the photometry of LH 118 as a function of magnitude.

Two of the stars for which we have CCD data also have been observed photoelectrically, and are also given in Table VII. In order to calibrate his photographic photometry, Lucke (1972) obtained *UBV* photoelectric photometry of several of the brighter stars in the region; unfortunately, the only star in common is that for LH 117-103 = LH 118-012 discussed above, which is Lucke's number 3. Our measurement of LH 118-012 is in reasonable agreement with Lucke's photometry. Our star LH 117-016 is Sk −70°116 (Sanduleak 1969), which is number 391 in the catalog of Ardeberg

TABLE VI. Photometric errors.

Mag	σ
<16.5	0.010
16.5–17.0	0.020
17.0–17.5	0.025
17.5–18.0	0.030
18.0–18.5	0.040
18.5–19.0	0.050
>19.0	0.090

et al. (1972), who obtained *UBV* photoelectric photometry. Here the agreement is also good.

Finally, in Table VII we compare our CCD measurements with the iris photographic measurements made by Lucke (1972) for stars in LH 117 and LH 118. This comparison is shown graphically in Fig. 9. For well-measured stars, the agreement is really quite excellent between Lucke's photographic work and our CCD work, with the differences in V scattering about zero with an amplitude of a few tenths of a magnitude. There appears to be a systematic difference in the $B-V$ color of 0.1, in the sense that our photometry is redder. However, it is also clear from Fig. 9 that the stars for which Lucke describes his photometry as "poor," or in which a double or multiple image was measured, can differ significantly from our CCD values.

In order to isolate the most massive *unevolved* stars, we first computed a reddening-free index $Q=(U-B)-0.72\times(B-V)$ using the photometry in Tables IV and V. All stars with $Q\leqslant -0.70$ and $V<17$ are listed in Tables VIII and IX. We give in Figs. 10 and 11 [Plates 15 and 16] the identification of just these stars in LH 117, and in Figs. 12–14 [Plates 17–19] for LH 118.

b) Other Imaging

LH 117 lies within the emission region Henize 180, also known as DEM 323 (Davies, Elliot, and Meaburn 1976). This nebulosity can be seen faintly in Fig. 1. According to Kennicutt and Hodge (1986), its Hα luminosity is ranked twenty-fifth of the $\approx$300 LMC H II regions for which they have measured Hα fluxes. During an observing run on the CTIO 0.9 m in November 1987, we obtained images of LH 117 in Hα and [O III]. Due to cloudy conditions, the data could not be calibrated into flux units, but we reproduce the Hα frames in Figs. 15 and 16 [Plates 20 and 21] to show the morphology of the excited gas.

c) Spectroscopy

Classification spectra were obtained for many of the stars in Tables VIII and IX using the CTIO 4 m telescope on the nights of (UT) 2–3 January 1988. A coated GEC CCD in an air Schmidt camera was used on the RC spectrograph with a 632 lines/mm grating (KPGL1) blazed at λ 4200. Wavelength coverage was from λ 3950 to λ 4750, with 2.5 Å resolution. Pixel-to-pixel gain variations were removed by dome-flat exposures of the "punto blanco" during the afternoon, and the underlying bias structure was removed by averaging multiple bias exposures made daily. Exposures of bright-sky twilight showed no detectable difference in the slit function compared to the dome flats. As the GEC chip suffered from a high incidence of radiation events, integrations longer than 10 min were made in three equal pieces, and then median filtered. A typical exposure of a 15th magnitude star required 10 min to reach a signal-to-noise of 70 per spectral-resolution element. Exposures of a He–Ar lamp were made at each new telescope position. The data were sky subtracted, extracted, and wavelength calibrated using the CTIO Sun workstation and IRAF.

Three of the stars in the photometry lists are bright ($V<13$) but *not* blue; two of these are so red ($B-V>1.5$) that they are good candidate red supergiants, e.g., LH 117-064 and LH 118-225. These stars had also been selected as red supergiant candidates from the Case objective-prism survey by Sanduleak and Philip (1977), although they had not been observed by Humphreys (1979) or Elias, Frogel, and Humphreys (1985). Spectra were obtained of all three using the CTIO (Yale) 1 m telescope on the night of (UT) 7 January 1988. The "2*D*-Frutti" two-dimensional photon-counting array was used with grating 47 (831 lines/mm) in second order, providing wavelength coverage from λ 3750 to λ 5000 at 1.5 Å resolution. Darks and flatfield exposures were made each day, and then summed before reducing the data. These 2*D*-Frutti data were reduced in a way similar to the GEC data, using the KPNO Sun workstation in Tucson.

The classification of these spectra was straightforward. Spectrum standards were compared to the program-star spectra, and for the later-type stars recourse was made to the Jacoby, Hunter, and Christian (1984) digital spectral atlas, and to Jaschek and Jaschek (1987). For the O stars, the classification comes primarily from the ratio of He I to He II, most notably the λ 4471 and λ 4542 lines. The ratio of the equivalent widths of these lines was compared to the compilation by Conti and Alschuler (1971). For the early B stars, more reliance was placed upon the spectral standards, which came from Garrison, Hiltner, and Schild (1977). We also utilized digital spectra of B type supergiant standards taken on the CTIO 1 m telescope plus 2*D*-Frutti by Dr. Ed Fitzpatrick. For these B stars, our classifications were based primarily on the relative strengths of Si II, III, and IV. The spectral types were determined independently by CDG and PM, and were generally in agreement within one subtype. These spectral types are given in Tables VIII and IX for the blue stars. Six of the stars had previously been classified by Conti, Garmany, and Massey (1986) from photographic plates; the classification of three of these stars was rediscussed by Garmany and Walborn (1987) from the same plate material. The B supergiant Sk $-70°116$ was classified as B2 I by Ardeberg *et al.* (1972), and we are in agreement with this.

In Table X we give the spectral types of the three bright late-type stars for which we obtained spectra. LH 117-064 (Case 62-4) is likely a supergiant, given the strength of Ca I λ 4226, and the relative strength of Sr II λ 4215 to Fe I λ 4263, and the relative strength of Fe I λ 4376 to Fe I λ 4383. The presence of strong TiO bands demonstrates that this star is of type M, and the relative strengths of the bands at λ 4584 and λ 4761 suggest a type of M2, although we cannot exclude the possibility that it is as late as M4. Nebular [O III] and Balmer emission are superposed upon the stellar spectrum, shown in Fig. 17.

LH 118-225 (Case 62-8) is of somewhat earlier type, with only a hint of TiO at λ 4954; the ratio of the barely resolved Cr I λ 4254 to Fe I λ 4250, and its overall appearance, suggest a late K type. We call it K5–M0. The spectrum is shown in Fig. 18. Although this spectrum is noisier than that of LH 117-064, the appearance of Ca I λ 4226 suggests that this

TABLE VII. Comparison of photometry.

a) Comparison Between CCD Measures of LH117 and LH118

Star	V	U-B	B-V
LH117-103	13.50	-0.87::	-0.12::
LH118-012	13.53	-1.00	-0.08
LH117-90	15.00	-0.74	-0.14
LH118-04	15.00	-0.73:	-0.07:

b) Comparison With Photoelectric Measurements

	CCD Measures			Photoelectric Measures			
Star	V	U-B	B-V	V	U-B	B-V	Reference
118-012	13.53	-1.00	-0.08	13.54	-0.95	-0.05	Lucke (1972)
117-016	12.09	-0.70	0.08	12.05	-0.72	+0.11	Ardeberg et al (1972)

c) Comparison With Lucke's (1972) Iris Photometry

1) LH117

Lucke #	CCD#	Iris		CCD		Comments
		V	B-V	V	B-V	
3	103	13.48	-0.14	13.50	-0.12::	Also LH118-012
8	223	15.57	-0.28	16.11::	0.20::	Lucke "poor"
9	217	15.80	1.03	15.71	1.05::	
10	212	14.97	0.53	14.94	0.67:	
11	214	13.15	-0.36	13.29	-0.19	
12	206	14.51	-0.48	15.06	-0.18	Lucke "poor"
13	187	14.24	-0.15	14.61	-0.14:	
14	197	14.57	-0.23	15.10	-0.15	Lucke "poor"
15	184	15.71	-0.30	15.97	-0.04:	
16	152	13.80	-0.15	14.03	-0.09	
17	168	15.26	-0.49	15.67	-0.17::	Lucke "double"
18	169	14.92	0.85	15.10	0.89:	
19	198	15.20	-0.27	15.47	-0.14	
20	191	15.80	-0.43	15.93	-0.11	
22	183	14.90	-0.31	15.08	-0.15	Lucke "double"
24	154	15.17	0.71	15.24	1.08::	Lucke "poor"
25	146	14.54	-0.14	14.75	0.02:	
26	131	15.53	-0.39	15.61	-0.17	
27	117	15.81	0.49	15.76	0.81:	
28	108	15.28	-0.18	15.77	-0.19	
29	106	14.32	0.76	14.52	0.85:	
30	98	14.77	-0.19	14.94	0.02	Lucke "double"
31	67	14.79	-0.27	15.50	-0.15	Lucke "double"
32	90	14.90	-0.27	15.00	-0.14	Also LH118-004
33	55	15.29	-0.46	16.04	-0.14::	CCD multiple
34	43	13.70	-0.11	14.08	-0.18	Lucke "poor"; CCD multiple
35	19	15.07	-0.15	15.25	-0.12	
36	16	12.03	-0.04	12.09	0.08	
37	14	14.63	-0.06	14.69	-0.05	
38	64	12.83	1.62	12.67	1.71::	
43	118	11.79	-0.00	12.23	-0.11	CCD multiple

2) LH118

Lucke #	CCD#	Iris		CCD		Comments
		V	B-V	V	B-V	
1	241	13.34	-0.35	13.35	-0.23	
2	239	12.64	-0.22	13.23:	-0.20	CCD Multiple
3	234	15.56	-0.44	15.47:	-0.21	Lucke "double"
4	225	12.87	1.87	12.69	1.92::	
5	197	15.45	-0.30	15.39	-0.16	
6	138	13.98	-0.32	13.94::	-0.18::	
7	116	14.91	-0.31	14.90	-0.14::	
8	34	15.95	0.97	15.77	1.14::	
9	105	15.12	-0.29	15.00	-0.13:	
10	72	15.55	0.47	15.47	0.64:	Lucke "poor"
11	110	15.81	-0.16	15.83	-0.15::	Lucke "poor"
12	165	15.14	-0.36	15.14	-0.19	
13	162	15.75	1.44	15.85	1.63::	Lucke "double"
14	161	14.02	0.77	14.04	0.87:	
15	182	14.10	-0.31	13.88	-0.19	

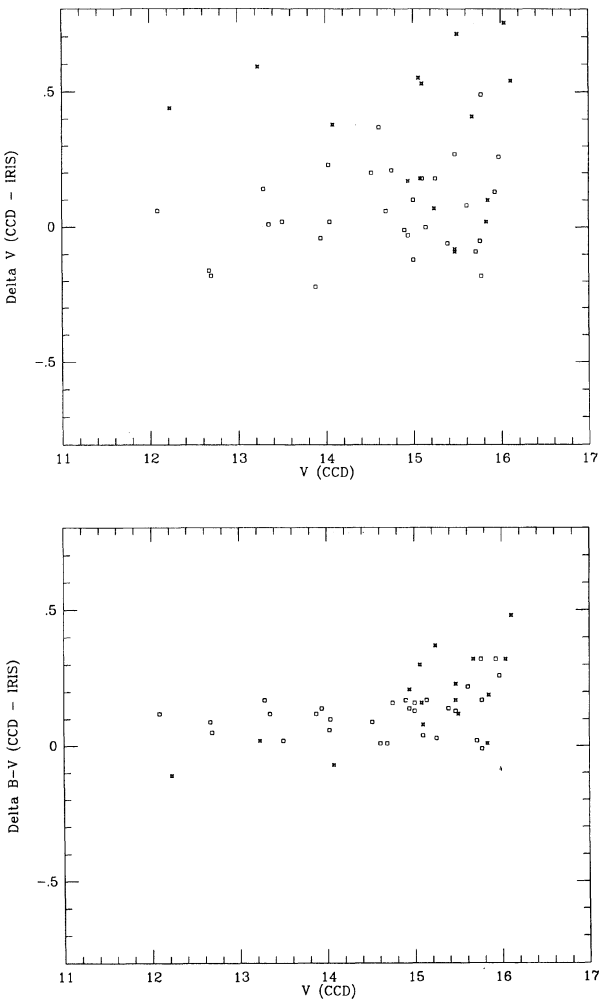

FIG. 9. Comparison of Lucke's (1972) iris photographic photometry with our CCD photometry. The starred symbols indicated the stars for which Lucke describes the images as "poor," "multiple," or "double," or for which it is clear from CCD data that they are several stars.

star is also likely a supergiant, although the spectroscopic evidence is weaker. We note, though, that the number of foreground Galactic stars this bright and this red that we would expect to appear in the ≈ 25 arcmin^2 covered by our CCD frames of LH 118 is < 0.1 (Ratnatunga and Bahcall 1985).

The star LH 118-071 is a foreground G dwarf. This is consistent with the model of Ratnatunga and Bahcall (1985), which predicts that one to two Galactic stars of such brightness and color might be expected to appear on our frames.

III. ANALYSIS

a) H–R Diagrams

The "observational" H–R diagrams (color–magnitude relations) are shown in Figs. 19 and 20. Our next step will be to transform to the theoretical plane (M_{bol} vs log T_{eff}), but first there are several comments worth making on the color–magnitude diagrams. We have plotted these both with $B - V$ and $U - B$ as the abscissa. In the $B - V$ plot most stars fall into a "blue plume." In the $U - B$ diagram, this plume resolves itself into the main sequence, demonstrating the usefulness of the U measures when dealing with hot stars. We have plotted with different symbols the stars for which we have good photometry and/or spectroscopy, and the stars for which the photometry is poorer; the stars with poor photometry will not be used in constructing the theoretical H–R diagram. Ratnatunga and Bahcall (1985) use their model of the Milky Way to predict the number of foreground stars in various magnitude and color bins towards Local Group galaxies including the LMC, and it is useful to consider this in interpreting Figs. 19 and 20 and what follows. In the region where $B - V < 0.8$, contamination will be insignificant; only a few stars are expected to be foreground, and these are likely to be the stars to the red of the blue plume. In the sparsely populated region for which $0.8 < B - V < 1.3$, the number of stars is consistent with their all being foreground, and in fact the model prediction matches the observed number remarkably well. For instance, using the area covered by the two CCD frames centered on LH 117, we would expect 0.3 stars in this color range with $13 < V < 15$, and we observe 1. In the range $15 < V < 17$, we expect 3.1 and we observe 5. In the range $17 < V < 19$, where incompleteness should begin to matter, their model predicts 7.5 and we observe 3. Similar results are obtained for the somewhat larger area observed for LH 118, and, as discussed above, the two stars tentatively identified as red supergiants fall in regions of the diagram highly unlikely to contain any foreground stars.

The photometry and spectroscopy discussed in the preceding sections can be used to derive temperatures and bolometric magnitudes for the stars in these two OB associations. Although for the most part the bluest stars have spectral types, the photometry provides most of the information for stars cooler than O9.

We first consider the reddening within LH 117 and LH 118. In Figs. 21 and 22 we show the two-color diagrams for the two associations, along with the intrinsic relation for early-main-sequence stars and supergiants. The reddening line for an O9.5 V star is indicated by a dashed line. We have cleaned these diagrams somewhat by restricting the dataset to stars whose photometric errors are less than 0.07 mag in $U - B$ and $B - V$ (compare with Figs. 19 and 20). By sliding the data along the reddening line, we arrive at a mean color excess $E(B - V) = 0.10$ for LH 117, and $E(B - V) = 0.08$ for LH 118. Our estimate of the error for these "eyeball" estimates is 0.02. Note that while a single average reddening seems to work adequately for LH 118 (Fig. 22), there are still a number of stars in LH 117 (Fig. 21) whose photometry suggests appreciably more reddening. This is what we expect based upon a comparison of the spectral types with the photometry in Table VIII: there appear to be variations in $E(B - V)$ throughout LH 117. This appears less true for LH 118 (Table IX), although there are fewer stars present. Figures 15 and 16 show that the Hα emission is very patchy, suggesting that the gas (and dust?) is not distributed uniformly. These values may be considered the "average minimum reddenings"; below, we will use a relation between the intrinsic color $(B - V)_0$ and a reddening-free parameter to derive slighly higher values for the average reddening.

For the stars without spectra, we will need to derive temperatures and bolometric corrections from their UBV colors. There are numerous discussions in the literature of the relation between temperature and $(B - V)_0$ (see Böhm-Vitense

TABLE VIII. Bluest stars in LH 117.

Star	1950 RA	1950 DEC	x	y	V	$U-B$	$B-V$	Q	Spectral Type New	Spectral Type Publ.	Comment
16	05 49 32.78	−70 03 20.0	106.1	178.0	12.09	−0.70	+0.08	−0.76	B2I	B2I	Sk−70° 116
118	05 49 19.78	-70 04 48.7	284.7	316.6	12.23	−0.92	−0.11	−0.84	—	O4:III(f)	Sk−70° 115
214	05 49 19.40	−70 06 23.6	207.1	258.5	13.29	−1.09	−0.19	−0.95	O3-4	O3-4	
103	05 49 49.62	−70 04 25.8	244.3	4.5	13.50	−0.87::	−0.12::	−0.79	O9.7	—	LH118-012
140	05 49 22.78	−70 05 05.8	52.3	216.5	13.52	−0.98	−0.11	−0.90	O3-4(f*)	O3III(f*)	
152	05 49 11.28	−70 05 19.3	75.3	336.3	14.03	−0.92	−0.09	−0.86	—	O7V	
43	05 49 39.12	−70 03 54.5	178.1	113.0	14.08	−0.99	−0.18	−0.86	O6V	O6V	
187	05 49 09.37	−70 05 51.0	138.1	358.9	14.61	−0.95:	−0.14:	−0.85	O9V	late O	
14	05 49 24.57	−70 03 20.4	105.2	263.8	14.69	−0.88	−0.05	−0.84	O6.5((f))	—	
62	05 49 21.67	−70 04 02.9	191.3	295.4	14.73	−0.84	−0.12	−0.76	O9V	—	
146	05 49 18.69	−70 05 09.4	58.0	259.0	14.75	−0.87:	+0.02:	−0.88	—	—	early B?
98	05 49 27.76	−70 04 24.4	236.7	232.6	14.94	−0.88	+0.02	−0.90	O9	—	
206	05 49 12.56	−70 06 15.1	187.6	328.2	15.06	−0.93	−0.18	−0.80	O8	—	
183	05 49 25.06	−70 05 46.6	134.9	196.8	15.08	−0.96	−0.15	−0.86	O9	—	
197	05 49 14.40	−70 06 04.9	167.8	308.3	15.10	−0.89	−0.15	−0.79	B0	—	
144	05 49 00.76	−70 05 11.5	56.0	444.1	15.23	−0.80::	+0.00::	−0.80	O9	—	
19	05 49 34.73	−70 03 27.0	120.8	157.9	15.25	−0.79	−0.12	−0.71	O9.5	—	
198	05 49 20.91	−70 06 04.6	169.6	241.2	15.47	−0.89	−0.14	−0.79	B0	—	
67	05 49 35.35	−70 04 06.1	200.8	152.8	15.50	−0.88	−0.15	−0.78	—	—	
131	05 49 26.61	−70 04 58.7	39.4	176.4	15.61	−0.95	−0.17	−0.83	B0+EMS	—	
80	05 49 20.98	−70 04 11.1	208.1	302.9	15.66	−0.80::	−0.07::	−0.76	—	—	
168	05 49 19.29	−70 05 36.5	112.6	255.3	15.67	−0.94::	−0.17::	−0.82	—	—	mid B?
73	05 49 20.46	−70 04 09.9	205.4	308.3	15.70	−0.81:	−0.14:	−0.71	—	—	
108	05 49 25.63	−70 04 41.0	270.2	255.3	15.77	−0.88	−0.19	−0.74	B2	—	
137	05 49 21.76	−70 05 03.0	46.2	226.8	15.83	−0.86	−0.06	−0.82	—	—	
224	05 49 21.42	−70 07 01.3	283.5	241.2	15.94	−0.84	−0.13	−0.75	—	—	
184	05 49 13.83	−70 05 49.1	136.0	312.8	15.97	−0.81:	−0.04:	−0.79	—	—	mid B?
31	05 49 38.62	−70 03 46.7	162.0	118.0	16.01	−0.88	−0.18	−0.76	—	—	
55	05 49 34.41	−70 03 58.7	185.6	162.3	16.04	−0.91::	−0.14::	−0.82	—	—	
51	05 49 21.16	−70 03 59.0	183.4	300.7	16.10	−0.92::	−0.05::	−0.88	—	—	
119	05 49 18.57	−70 04 48.8	284.6	329.2	16.10	−0.88::	−0.12::	−0.79	—	—	
223	05 49 08.67	−70 06 50.3	257.0	371.5	16.11::	−0.82::	+0.20::	−0.96	—	—	OB+EMS
188	05 49 30.20	−70 05 47.8	139.2	143.9	16.13	−0.91::	−0.11::	−0.83	—	—	
186	05 49 29.70	−70 05 47.4	138.2	149.0	16.15	−0.78::	−0.05::	−0.75	—	—	
128	05 49 29.34	−70 04 56.0	34.9	147.9	16.22	−0.82	−0.12	−0.73	—	—	
135	05 49 23.16	−70 05 00.0	40.8	212.1	16.23	−0.87:	−0.12:	−0.79	—	—	late O?
82	05 49 22.65	−70 04 13.2	212.7	285.6	16.28	−0.85	−0.12	−0.76	—	—	
99	05 49 28.72	−70 04 25.7	239.5	222.6	16.37	−0.86	−0.10	−0.78	—	—	
143	05 49 22.58	−70 05 07.1	54.8	218.7	16.47::	−0.87::	+0.02::	−0.89	—	—	
165	05 49 36.75	−70 05 27.1	100.0	74.5	16.48	−0.87::	−0.12::	−0.78	—	—	
30	05 49 41.40	−70 03 45.2	159.5	88.9	16.52	−0.86	−0.16	−0.74	—	—	
29	05 49 05.98	−70 03 47.4	156.5	458.8	16.53	−0.84	−0.15	−0.73	B2	—	
159	05 49 22.82	−70 05 24.8	90.3	217.9	16.58	−0.84::	−0.15::	−0.74	—	—	
15	05 49 27.59	−70 03 20.1	105.3	232.3	16.60	−0.78	−0.04	−0.75	—	—	
66	05 49 35.38	−70 04 04.1	196.8	152.4	16.64	−0.88::	−0.14::	−0.78	—	—	
151	05 49 23.71	−70 05 15.8	72.7	207.9	16.71	−0.80	−0.05	−0.76	—	—	
110	05 49 23.50	−70 04 42.6	272.9	277.6	16.72	−0.82	−0.16	−0.71	—	—	
134	05 49 17.53	−70 05 01.0	40.8	270.2	16.77	−0.80	−0.09	−0.74	—	—	
120	05 49 26.19	−70 04 49.4	287.4	249.8	16.83	−0.84	−0.13	−0.75	—	—	
92	05 49 09.81	−70 04 21.0	226.0	419.8	16.89	−0.80	+0.03	−0.82	—	—	
91	05 49 19.22	−70 04 20.0	225.8	321.6	16.92	−0.81	−0.01	−0.80	—	—	
49	05 49 34.57	−70 03 56.8	181.6	160.6	16.98	−0.89::	−0.11::	−0.81	—	—	

Note: Stars 1-128 are on Fig. 10; 129-235 on Fig. 11

1981), but at least for O and B type stars a better relation is between temperature and $(U-B)_0$, since the change in $(B-V)_0$ is quite small with temperature for stars this hot. However, the discussion above indicates that we cannot adopt a single value for $E(B-V)$ or $E(U-B)$, and for that reason we chose instead to use Q, the reddening-free parameter defined above.

If we examine the intrinsic colors given by FitzGerald (1970), we find that the relation between Q and $(B-V)_0$ (and hence effective temperature) is single valued as we proceed down the main sequence until we get to early A type stars, after which it is not. Using the effective-temperature calibration given by Flower (1977) with the intrinsic color relations listed by FitzGerald (1970), we derive

TABLE IX. Bluest stars in LH 118.

Star	1950 RA	1950 DEC	x	y	V	$U-B$	$B-V$	Q	Sp. Type	Comment
239	05 50 09.74	−70 09 00.7	157.3	188.6	13.23:	−0.82	−0.20	−0.68	O9	Blended with 240
241	05 50 12.59	−70 09 01.5	159.0	161.8	13.35	−0.89	−0.23	−0.73	O5	
12	05 49 49.83	−70 04 25.3	34.8	420.5	13.53	−1.00	−0.08	−0.95	O9.7	LH117-103
182	05 49 51.90	−70 07 18.8	162.4	400.3	13.88	−1.00	−0.19	−0.86	O9III	
138	05 50 14.89	−70 08 06.6	265.7	164.0	13.94::	−0.89::	−0.18::	−0.77	B1	
240	05 50 10.00	−70 09 01.1	158.1	186.2	14.10::	−0.99::	−0.16::	−0.88	—	Blended with 239
116	05 50 16.73	−70 05 56.7	224.2	141.5	14.90	−0.87::	−0.14::	−0.77	B2	
105	05 50 10.72	−70 05 48.8	207.1	203.8	15.00	−0.91::	−0.13::	−0.82	B0	
165	05 50 01.11	−70 06 53.3	112.3	303.7	15.14	−0.93	−0.19	−0.80	O9	
230	05 50 08.90	−70 08 26.7	87.2	196.3	15.56	−0.85:	−0.21:	−0.70	—	
154	05 50 09.51	−70 06 37.1	80.9	215.9	15.82	−0.89::	−0.15::	−0.79	—	
78	05 50 09.61	−70 05 28.1	165.1	215.2	15.82:	−0.88	−0.09:	−0.82	—	
110	05 50 05.09	−70 05 51.9	212.1	262.3	15.83	−0.92::	−0.15::	−0.81	B1	
169	05 50 10.84	−70 06 55.7	119.3	202.3	15.84	−0.81:	−0.16:	−0.70	—	
20	05 50 26.75	−70 04 26.0	43.8	36.8	15.84	−0.85::	−0.14::	−0.75	—	
222	05 50 17.30	−70 08 17.6	288.8	139.5	15.85	−0.88::	−0.19::	−0.75	—	
211	05 50 18.50	−70 07 54.1	240.8	126.0	16.06	−0.85::	−0.18::	−0.73	—	
93	05 50 29.67	−70 05 38.4	190.2	7.1	16.30	−0.87::	−0.13::	−0.78	—	
98	05 50 12.26	−70 05 44.4	198.5	187.8	16.43	−0.89::	−0.11::	−0.82	—	
216	05 50 02.07	−70 08 05.2	259.8	296.8	16.44	−0.85::	−0.13::	−0.76	—	
76	05 50 08.31	−70 05 27.6	163.9	228.8	16.44	−0.83::	−0.14::	−0.74	—	
91	05 50 25.05	−70 05 37.7	187.7	55.0	16.55	−0.78::	−0.07::	−0.73	—	
86	05 49 46.74	−70 05 38.2	181.0	452.7	16.57	−0.82::	−0.08:	−0.76	—	
82	05 50 09.45	−70 05 33.2	175.4	216.9	16.85	−0.87::	−0.11::	−0.79	—	

Note: Stars 1-152 are on Fig. 12; 153-226 on Fig. 13; Stars 227-244 on Fig. 14.

$$\log T_{\rm eff} = 3.994 - 0.267Q + 0.364Q^2$$

for main-sequence stars with $(B-V)_0 < 0.00$. We will apply this equation to stars with $B-V < 0.15$, which in these associations corresponds approximately to $(B-V)_0 < 0.00$.

This transformation will take care of the majority of the stars, but there are a handful of redder stars for which we must find effective temperatures. Admittedly, most of these will be foreground stars (as discussed below), but a few of the lower-mass main-sequence stars will also fall into this category. (A main-sequence star with $(B-V)_0 = 0$ corresponds to $\approx 3\mathcal{M}_\odot$.) In order to provide good continuity with the bluer stars, we will first reconsider the matter of reddening using Q. From FitzGerald's (1970) intrinsic color relations, we find that

$$(B-V)_0 = 0.273(U-B)_0 - 0.008$$

for main-sequence stars of type A0 and earlier, and hence

$$(B-V)_0 = 0.330Q - 0.017, \quad (B-V)_0 < 0.00\,.$$

We can use this last equation, then, to derive the color excess $E(B-V)$ in a star-by-star manner for the bluer stars. For the stars with good photometry, we find that the most probable color excess $E(B-V)$ is 0.12 for LH 117, and 0.10 for LH 118. (These are a little higher than the values derived from the two-color diagram, which as expected provides essentially the "average minimum reddening," given how the "eyeball" fits were made.) Thus, for the few stars for which $(B-V) > 0.15$ we will compute $(B-V)_0$ from these somewhat higher values of the average reddening, and then use the effective-temperature scale of Flower (1977) as follows:

$$\log T_{\rm eff} = 3.99 - 0.510(B-V)_0,$$

$$0.0 < (B-V)_0 < 0.2\,,$$

valid for main sequence and giants,

$$\log T_{\rm eff} = 3.960 - 0.344(B-V)_0,$$

$$0.2 < (B-V)_0 < 0.5\,,$$

valid for all luminosity classes, and

$$\log T_{\rm eff} = 3.904 - 0.222(B-V)_0, \quad 0.5 < (B-V)_0$$

TABLE X. Other stars with spectroscopy.

Star	1950 RA	1950 DEC	x	y	V	$U-B$	$B-V$	Sp. Type	Comment
117-064	05 49 10.21	−70 04 06.2	194.9	414.8	12.67	2.23::	1.71::	M2I	Case 62-4
118-071	05 49 46.06	−70 05 25.2	154.4	459.8	12.22	0.29	0.60	GV	Foreground
118-225	05 50 01.26	−70 08 22.7	295.3	305.9	12.69	2.69::	1.92::	K5-M0I	Case62-8

Note: 117-064 is on Fig. 10, 118-071 is on Fig. 12, and 118-225 is on Fig. 13.

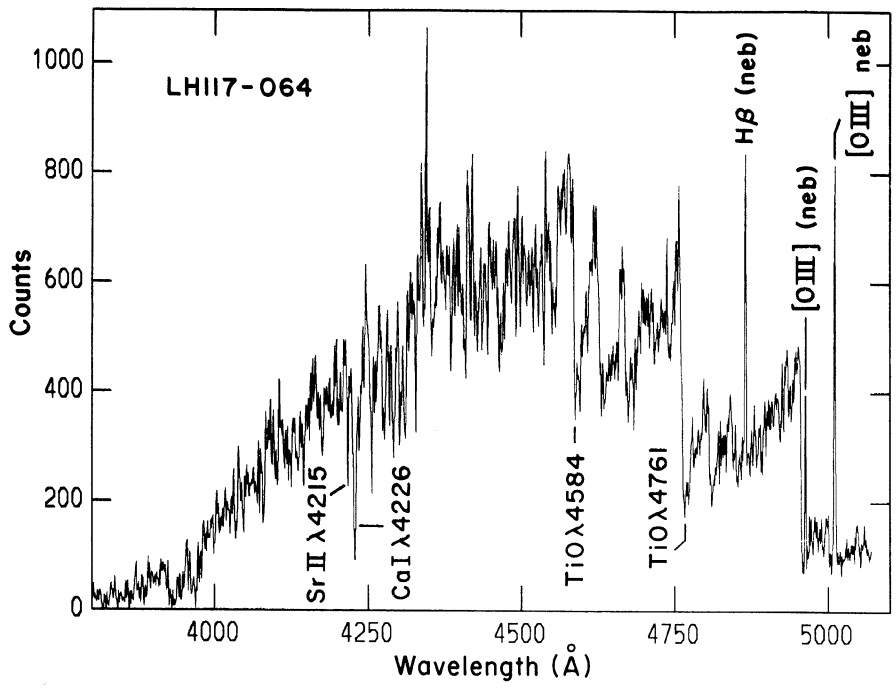

FIG. 17. Spectrum of LH 117-064, an M2 I supergiant. Note the TiO bands and the strong nebular lines.

for giants and supergiants.

Next, we will derive the absolute bolometric magnitudes for the stars without spectra:

$$M_{\rm bol} = V - A_V + {\rm BC} - 18.3\,.$$

We assume that the absorption A_V is $3.1 \times {\rm E}(B-V)$, where we compute ${\rm E}(B-V)$ from Q as described above for stars with $B-V<0.15$, and use the mean reddenings given above for the redder stars. We somewhat arbitrarily adopt a true distance modulus to the LMC of 18.3.

We will use bolometric corrections (BC) as a function of temperature derived from Flower's calibration:

$${\rm BC} = 23.493 - 5.926 \log T_{\rm eff}, \quad 4.5 > \log T_{\rm eff} > 4.0$$

and

$${\rm BC} = -207.075 + 107.390 \times \log T_{\rm eff} - 13.919 (\log T_{\rm eff})^2,$$
$$4.0 > \log T_{\rm eff} > 3.6\,.$$

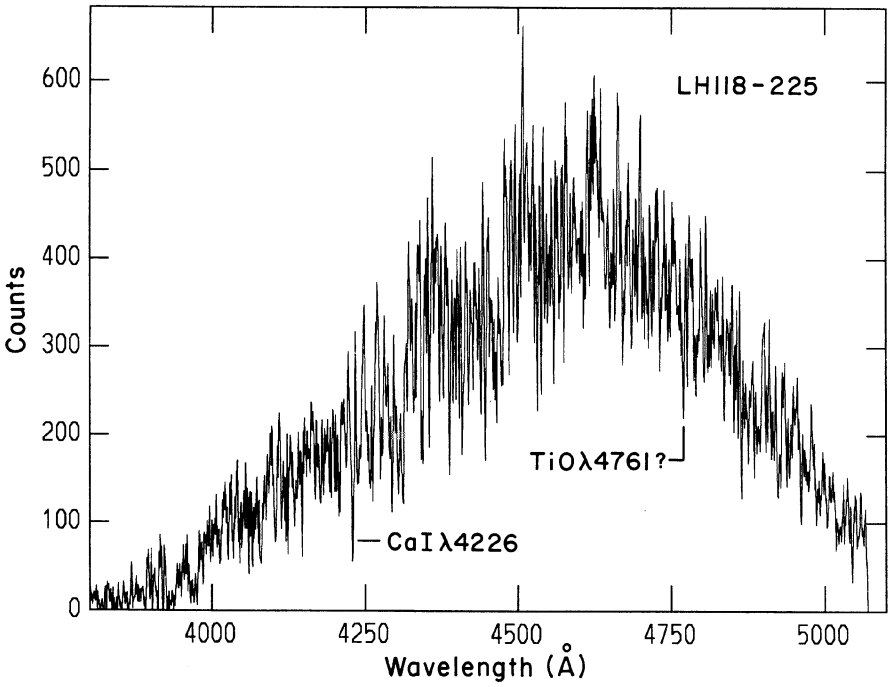

FIG. 18. Spectrum of LH 118-225, which we have tentatively identified as a K5–M0 I supergiant. Note by comparison with Fig. 17 the lack of TiO bands.

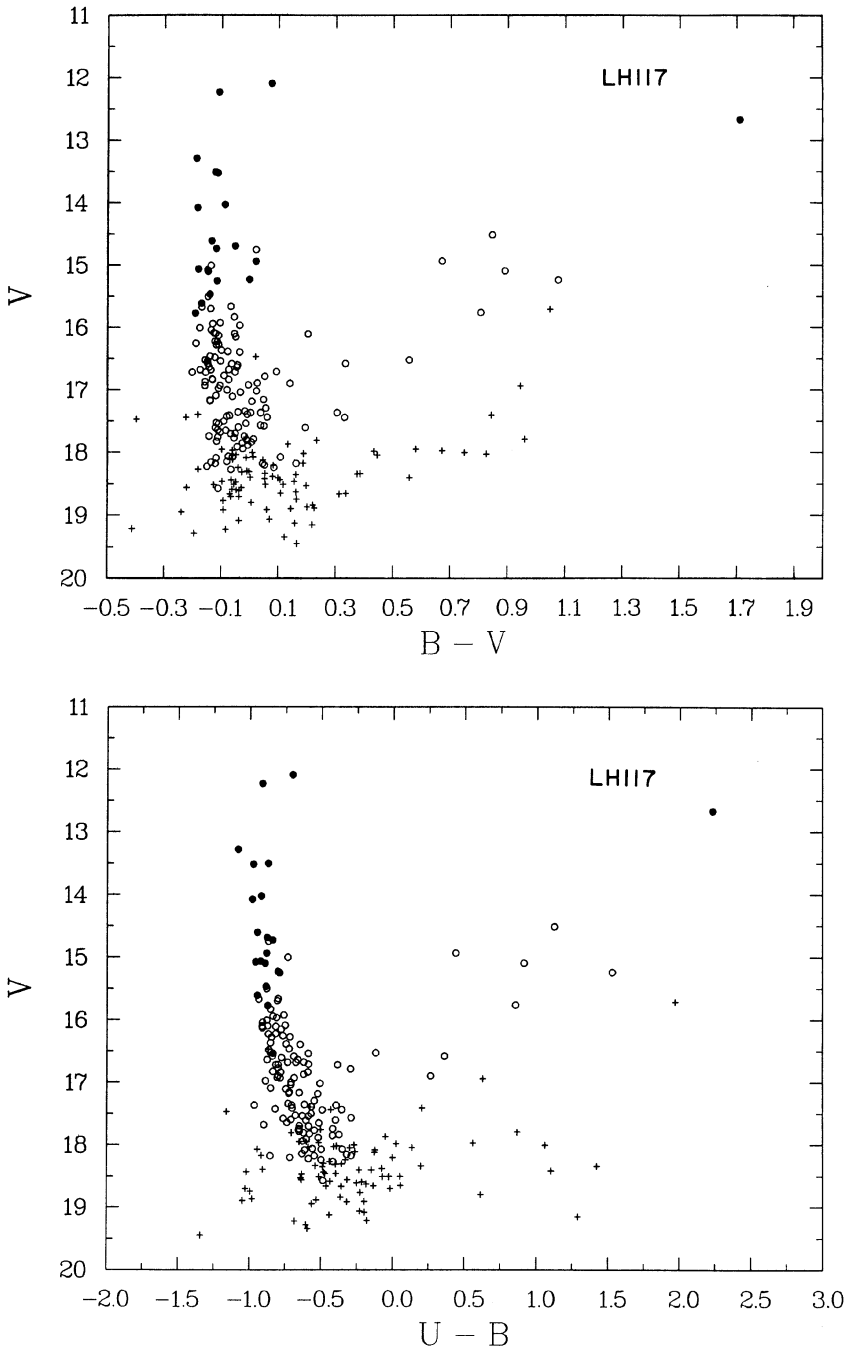

FIG. 19. Color–magnitude diagrams of LH 117. Dark circles denote the stars for which we have spectra, light circles show the stars for which we have "good" photometry (errors 0.07 mag or less), and the " + " symbols show the stars that have larger errors in their photometry.

The stars with spectra in Tables VIII and IX and the two late supergiants in Table X were assigned temperatures and bolometric corrections based on their spectral types. For the B type stars we used the effective-temperature scale and bolometric corrections given by Flower (1977), making use of the analytical approximations given above for the main-sequence stars, and using the tabulated value for the B supergiant. For the O type stars we used the recent calibration given in Chlebowski and Garmany (in preparation), which is based on work by Kudritski, Simon, and Hamann (1983), Simon *et al.* (1983), Bohannan *et al.* (1986), and Voels *et al.* (1988). The absolute visual magnitudes were derived from the distance modulus and color excess, defined individually for each star from the difference between the intrinsic and observed colors. The choice of intrinsic colors has been discussed in Conti, Garmany, and Massey (1986): we have used $(B-V)_0 = -0.30$ for the O stars and FitzGerald's (1970) colors for the B stars.

For the two red supergiants, we adopt the mean color excesses discussed above, as our photometry will not be sufficiently reliable for stars this red to derive $E(B-V)$ directly. For the M2 I star LH 117-064, we adopt $\log T_{\rm eff} = 3.53$ and

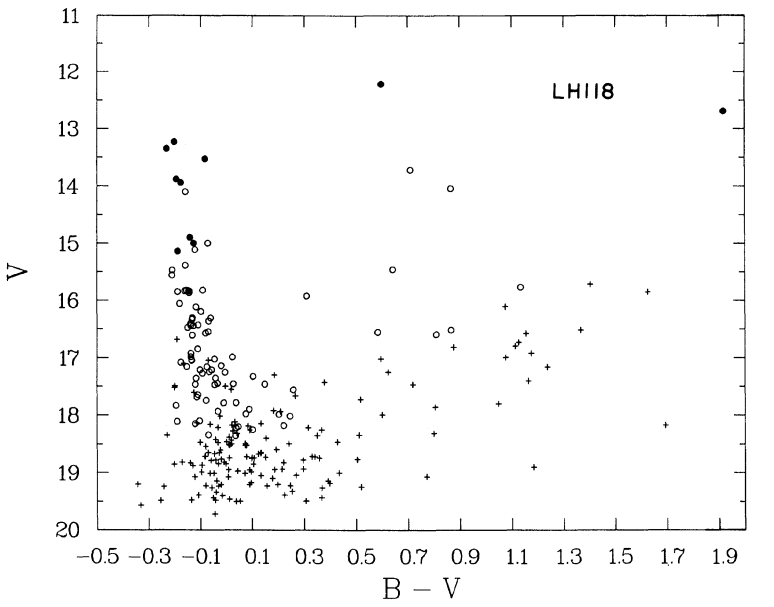

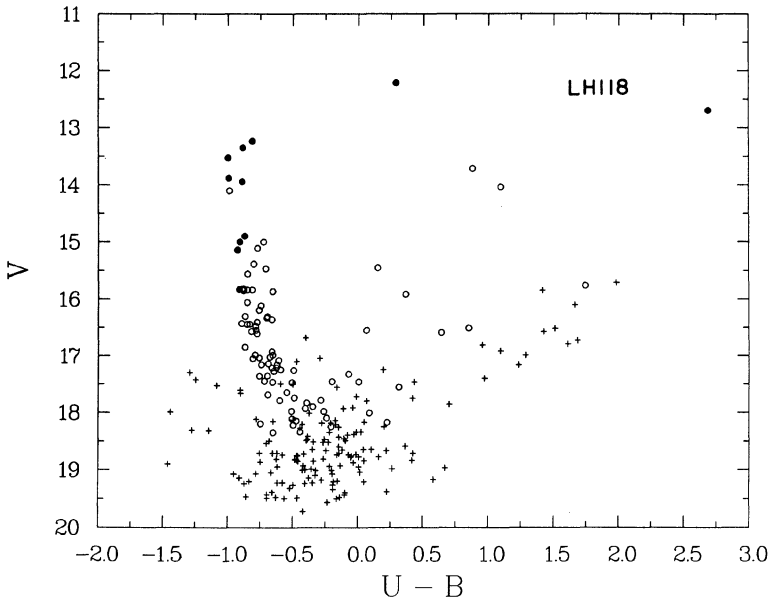

FIG. 20. Same as Fig. 19 for LH 118.

a bolometric correction of − 1.5 mag. For the "K5–M0" star LH 118-225 we adopt log $T_{\rm eff} = 3.57$ and a bolometric correction of − 1.0 mag, following Humphreys and McElroy (1984).

We list in Tables XI and XII the most luminous stars in each of these associations ($M_{\rm bol} < -6.0$, corresponding to $\approx 15 M_{\odot}$). We see that there are only a few of these stars for whcih we are missing spectral types, and that the number of luminous stars in LH 117 is about twice that found in LH 118. We shall show in the next section that this trend continues to lower masses.

We can now construct the "theoretical" H–R diagram for each association. These are shown in Figs. 23 and 24, where we have again used only those stars with spectroscopy or "good" photometry—in other words, every star not marked with a cross in Figs. 19 and 20. The evolutionary tracks by Maeder and Meynet (1987) and Maeder (1988) are also shown. These tracks are computed with a heavy-element content $Z = 0.02$; a more appropriate value for the LMC would be about half that (Lequeux *et al.* 1979; Dufour 1984), but there does not exist a complete set of evolutionary models over the mass range of interest here with the appropriate Z. The effect of lower metallicities on the evolutionary tracks will be to shift the ZAMS to slightly higher effective

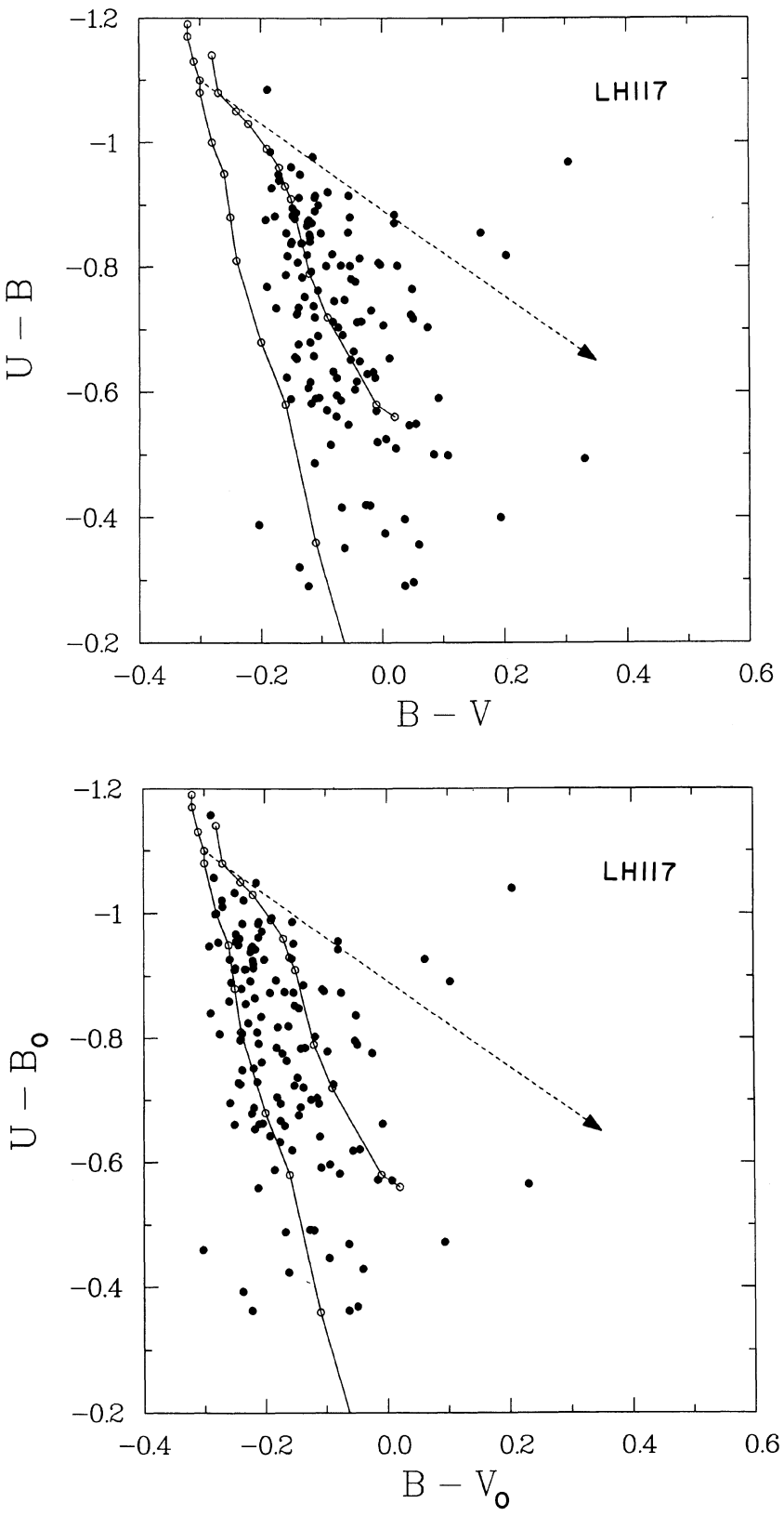

FIG. 21. Two-color relation for the stars in LH 117. The light circles connected by solid line segments show the intrinsic colors for main-sequence and supergiant stars given by Fitz-Gerald (1970). The dashed line shows the reddening line for an O9.5 V star. The solid points show the stars with "good" photometry. The second plot shows the same relation but with the stars shifted along the reddening line by E($B - V$) = 0.10.

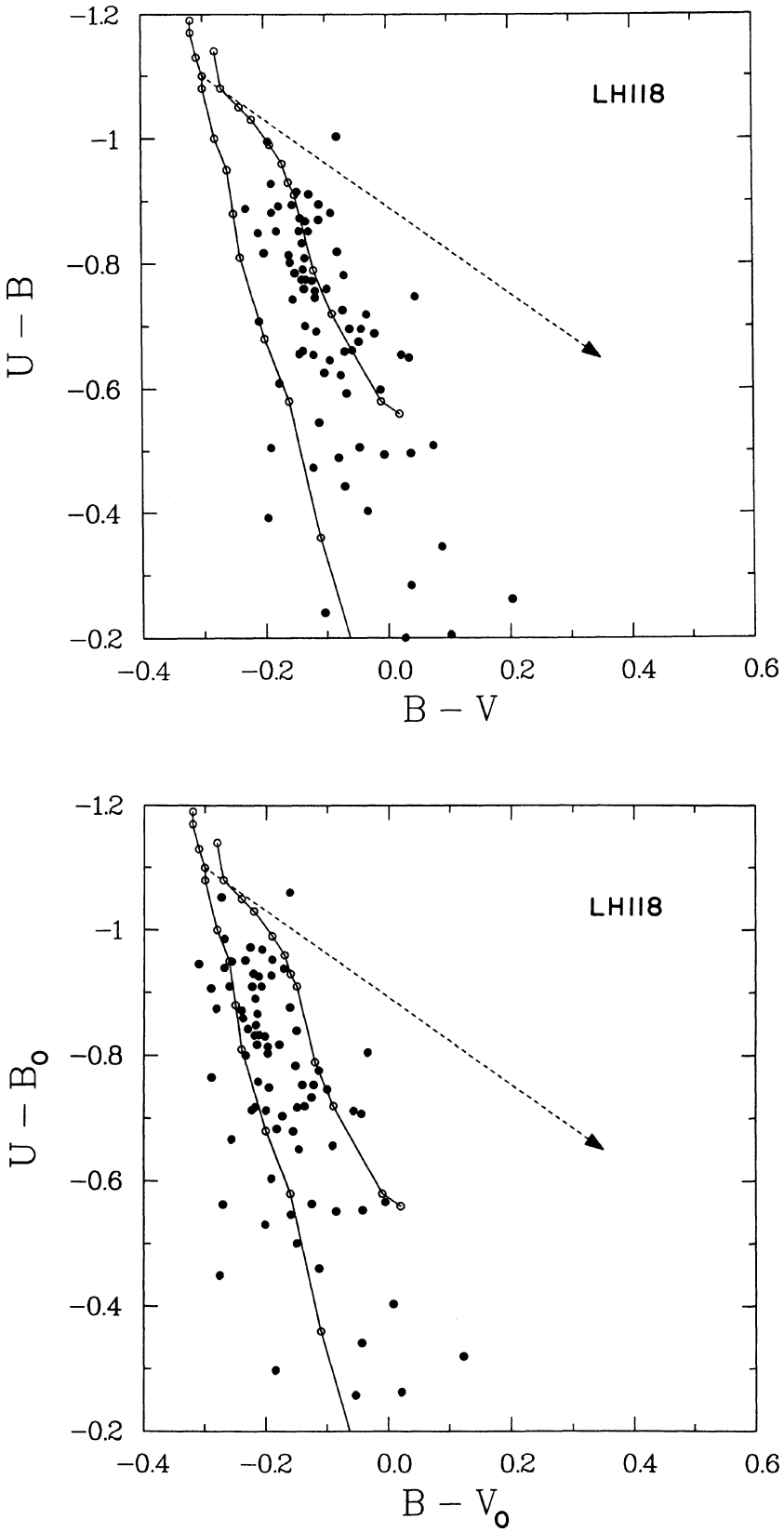

FIG. 22. Same as Fig. 21 for LH 118. The second plot shows the data shifted by E($B - V$) = 0.08.

TABLE XI. The most luminous stars in LH 117.

Star	Log T_{eff}	M_{bol}	$E(B-V)$	Sp. Type	Comment
118	4.65	-10.8	0.19	O4:III(f)	Sk-70° 115
214	4.68	-9.7	0.11	O3-4	
140	4.68	-9.7	0.19	O3-4	
16	4.29	-8.9	0.23	B2I	Sk -70° 116
152	4.60	-8.7	0.21	O7V	
43	4.62	-8.5	0.12	O6V	
103	4.48	-8.4	0.18	O9.7	LH118-012
14	4.62	-8.3	0.25	O6.5	
98	4.55	-7.8	0.32	O9	
146	4.51	-7.8	0.33	—	
187	4.55	-7.7	0.17	O9V	
62	4.55	-7.6	0.18	O9V	
144	4.55	-7.5	0.30	O9	
64	3.53	-7.4	0.10	M2I	
206	4.58	-7.2	0.12	O8	
183	4.55	-7.2	0.15	O9	
19	4.54	-7.0	0.18	O9.5	
197	4.47	-6.6	0.14	B0	
198	4.47	-6.3	0.15	B0	
137	4.46	-6.1	0.23	—	
51	4.50	-6.1	0.25	—	
131	4.47	-6.1	0.12	B0	

TABLE XII. The most luminous stars in LH 118.

Star	Log T_{eff}	M_{bol}	$E(B-V)$	Sp. Type	Comment
241	4.65	−9.3	0.07	O5	
239	4.55	−8.8	0.10	O9	
12	4.48	−8.4	0.18	O9.7	LH117-103
182	4.53	−8.1	0.11	O9III	
138	4.38	−7.1	0.07	B1	
165	4.55	−7.0	0.11	O9	
225	3.57	−6.9	0.08	K5-M0I	
105	4.47	−6.8	0.16	B0	
4	4.36	−6.1	0.17	—	
78	4.46	−6.0	0.19	—	

temperatures, but the size of the effect is quite small, about 0.01–0.02 dex, in going from $Z = 0.02$ to $Z = 0.01$ (Brunish and Truran 1982).

We find in Figs. 23 and 24 excellent agreement with the location of the ZAMS and the hottest stars. Most stars are located on the left half of the main sequence (the "squiggle" in the evolutionary tracks indicates the end of core-H burning). In interpreting these diagrams it is useful to remember the discussion at the beginning of this section, that the stars to the red of the "blue plume" in Figs. 19 and 20 are likely foreground Milky Way members. We have marked with an "F" the position of the foreground G star in Fig. 24, and expect the smattering of fainter stars with log $T_{\rm eff} \approx 3.8$–3.9 in Figs. 23 and 24 also to be foreground stars. Note that in going to the log $T_{\rm eff}$ abscissa the hot stars have been stretched out compared to their distribution in the $B-V$ or even the $U-B$ plane, but that the cool stars have been squeezed together: although the K5–M2 supergiant appears relatively near the foreground G star in Fig. 24, its $B-V$ color is much redder (cf. Fig. 22), and the star is much too red and too bright to be a likely foreground object.

The most noteworthy feature of the H–R diagrams is the

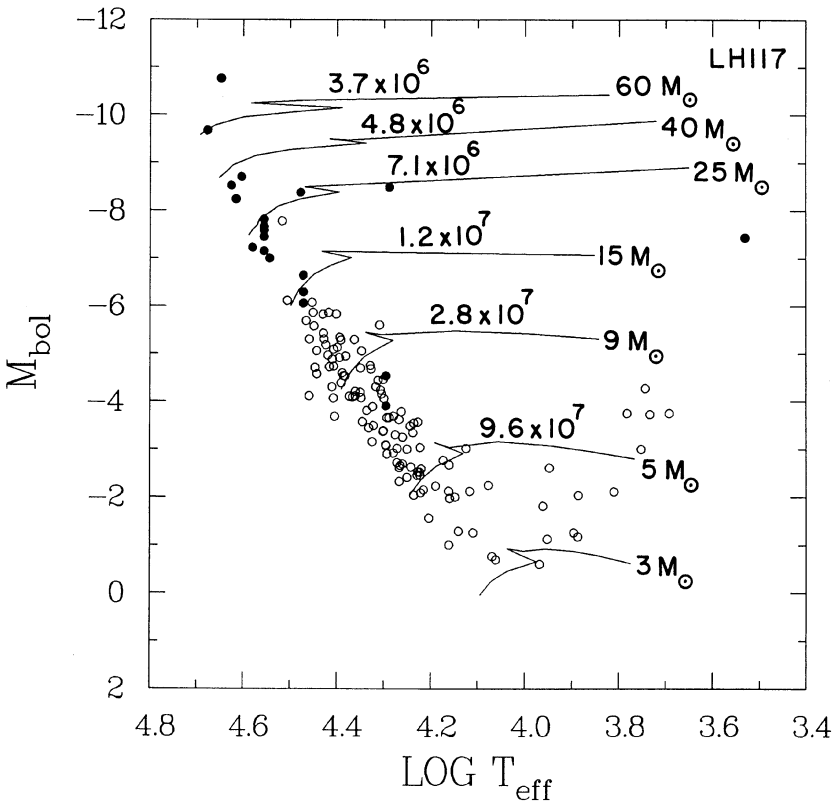

FIG. 23. H–R diagram for LH 117. The solid points denote the stars for which we have spectra, while the light circles are the stars for which we have good photometry. Evolutionary tracks from Maeder and Meynet (1987) and Maeder (1988) are indicated, along with their main-sequence lifetimes (corresponding to the squiggle in the tracks).

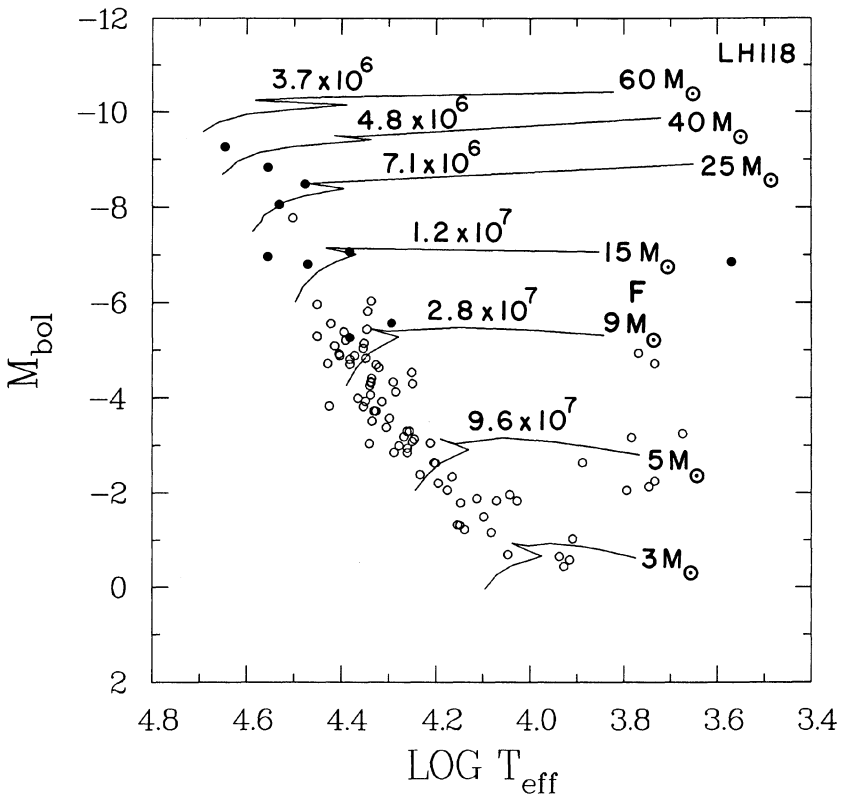

FIG. 24. Same as Fig. 23 for LH 118. We have marked the location of the foreground G dwarf star LH 118-071 with an "F."

evidence that the stars in these associations did not quite form coevally. Most of the stars are located quite close to the ZAMS, including stars of 40–60 $\mathcal{M}_\odot$. However, there are stars of lower mass (20–30 $\mathcal{M}_\odot$) that have *already* evolved to supergiants. This effect is probably even more pronounced than is evident in the figures, as studies of the field OB stars in the LMC (which should populate the entire mass sequence) show that the current set of evolutionary tracks does not extend sufficiently far to cooler temperatures; i.e., the actual main sequence is wider than the tracks indicate (Humphreys and McElroy 1984; Fitzpatrick and Garmany, in preparation).

Can these few supergiants be incorrectly placed? In the case of LH 118, the spectroscopic evidence that LH 118-225 is a red supergiant is not overwhelming; we have noted above that it is improbable that we would happen upon a foreground Galactic star this red and this bright in the small area covered by our CCD frames, but we cannot exclude the possibility. However, in LH 117 we have two evolved supergiants: the B2 I star Sk −70°116 (LH 117-016) and the M2 I star LH 117-064. In the case of LH 117-064, we have classified the star as M2 on the basis of the appearance of weak TiO bands. One can imagine that with the lower metallicity of the LMC we may be underestimating the temperature this way. However, Elias, Frogel, and Humphreys (1985) argue that this effect is small for the metallicity difference between the Galaxy and the LMC, amounting to less than half a subtype for early M stars, which would affect the bolometric correction by $\approx$0.1 mag (Humphreys and McElroy 1984). If we had misclassified this star, and it were actually as late as M4, then the bolometric correction would have been underestimated by 1 mag (Humphreys and McElroy 1984). However, we see from Table XII that this star is 3 mag fainter than the O4 giant, and 2 mag fainter than the O3–4 stars. Similarly, the B supergiant is 2 mag below that of the most luminous star, and 1 mag below the next two most luminous stars. While there may be some uncertainty in the exact bolometric correction to apply to a B supergiant (compare Humphreys and McElroy (1984) with Flower (1977)) this is unlikely to introduce an error greater than a few tenths of a magnitude, and we note that our spectral type and photometry agree with that of Ardeberg *et al.* (1972).

We have indicated in Figs. 23 and 24 the putative main-sequence lifetimes from the evolutionary models; we can see that the evolved supergiants have probably formed between 6 and 10 million years earlier than the majority of stars in these associations. The ages of the 30–60 $\mathcal{M}_\odot$ stars in Fig. 23 are 1 or 2 million yr if we simply adopt Maeder and Meylan's (1987) isochrones, but in any event must be less than the main-sequence lifetimes of 3 or 4 million yr. This is in contrast to the ages of the B and M supergiants, which must be at $7–12 \times 10^6$ yr old.

Herbst and Miller (1982) present definitive evidence of an appreciable age spread among the stars in the young galactic cluster NGC 3293, with the lower-mass stars forming first, and star formation proceeding over 20 million yr. This conclusion came about as NGC 3293 has a well-populated main sequence extending from late O type stars down through 1.5 $\mathcal{M}_\odot$; however, the contraction time for the lower-mass stars is 25 million yr, much greater than the lifetime of the late O stars present in the cluster. In our two associations, though, we see something more haphazard. Our photometry does not extend to faint enough limits to determine whether there is a background of lower-mass stars that may have

formed earlier than the massive stars that populate the main sequence. We note that the contraction time of a $5\mathcal{M}_\odot$ star is still very short (6×10^5 yr), and were our photometry to extend down to $1.5\mathcal{M}_\odot$ main-sequence stars, the confusion with the LMC background would be enormous, as can be inferred from the color–magnitude diagram for the LMC field stars in Flower *et al.* (1983). However, our data do show that star formation among the higher-mass stars was not completely coeval on the timescale of ≈10 million yr, but that a few 15–25 $\mathcal{M}_\odot$ stars must have formed first. Of course, some (or all) of the lower-mass stars could also have formed at this earlier time and would still be near the ZAMS given the longer time they spend on the main sequence. However, we can safely assume that not many stars of higher mass have formed earlier, as any star ending its life as a supernova would clear the region of gas, making further star formation very difficult.

There are a few hints in the literature that lead us to speculate that this situation is a common but generally unrecognized characteristic of Galactic OB associations as well. Humphreys, Nichols, and Massey (1985) show examples of several H–R diagrams of Galactic OB associations (their Fig. 1), and we can see the same effect in Tr 27 and Cyg OB1. We have made a very cursory examination of the $M_{\rm bol}$, log $T_{\rm eff}$ data for the stars in Galactic OB associations used in the study by Humphreys and McElroy (1984) (a machine-readable version of this containing the data for individual stars was kindly made available by Dr. R. Humphreys), and we find that this is more the rule than the exception: Ser OB1, Vul OB1, and Sgr OB1 all show this effect to greater or lesser degrees. With the thorough job of extracting spectral types and photometry from the literature already performed by Humphreys and McElroy (1984), we believe that the "coevality question" posed by our study here can be thoroughly answered for Galactic associations.

One complication in such a study is the possibility that spatially separated subgroups within "one" OB association may have formed at different times. As discussed by Blaauw (1964), there are several OB associations in which the earliest-type (and least evolved) stars are found in a concentrated section at one edge of the association, with the association becoming less condensed and further evolved at the other end. Nevertheless, that is not the case in LH 117 and LH 118, as far as we can tell. The two nearby, bright neighbors of the B2 I supergiant (LH 117-016) are the O6 star LH 117-043 and the O6.5 star LH 117-014, as can be seen in Figs. 2 and 10. Similarly, the M2 I supergiant LH 117-064 is relatively near the most luminous of the LH 117 stars, LH 117-118. In LH 118 the O5 star LH 118-241 is one of the nearest neighbors of the K5–M0 supergiant LH 117-225 (see Fig. 6).

b) The Initial Mass Function

We can use the data presented in the previous section to construct the initial mass function (IMF) for these two associations, although two caveats must be kept in mind. The first of these is that there are simply not very many stars here—in particular, the effect of small-number statistics for the upper mass bins will be quite severe. We can alleviate this somewhat by combining all the data for the two associations. Second, and this may well be a more troublesome effect, is the problem that we have just shown that the stars in the associations were not all born at the same time. We will restrict ourselves to stars on the main sequence only and ignore the supergiants in what follows, but in constructing the IMF for these associations we will have to assume that star formation was "instantaneous." This has the advantage over the construction of *field* or *composite* IMFs in that we will not have to correct for the relative ages of the stars populating the diagram (with the resulting uncertainty in the main-sequence lifetimes), but we are beginning with an assumption that we already know is not strictly true, although, as noted above, most of the main-sequence stars do fall near the ZAMS.

We have decided not to make any background corrections in our number counts for the following reason. We show in Figs. 2–6 every star for which photometry has been performed. A comparison with Fig. 1 will show that nearly all the stars bright enough to have been measured lie within the boundaries of the OB associations as drawn by Lucke (1972). Although a few stars—including a few of the more massive stars—occur outside the boundaries, even the faintest stars for which we have photometry occur very near the edge of the boundaries in these cases rather than towards the edge of the frame, say. We conclude that our data indicate that the boundaries as drawn are a little too small. Fitzpatrick and Garmany (in preparation) find much the same thing considering the "field" OB population of the clouds.

To construct the IMF, we first simply count the number of main-sequence stars between mass tracks in Figs. 23 and 24 and divide by the total area, which we take to be 8.8 kpc^2. Using Scalo's (1986) notation, the slope of the initial mass function is

$$\Gamma = d\log\xi(\log m)/d\log m\,,$$

where $\xi(\log m)$ is the mass function in units of number of stars born per unit logarithmic (base ten) mass interval per unit area. For a power law mass spectrum

$$f(m) = Am^{\gamma}\,,$$

the index $\gamma = \Gamma - 1$. (In Tinsley's (1980) notation, $x = -\Gamma$.)

We give in Table XIII the number of stars in each mass range, and the number per kpc^2 per unit log mass interval ($\xi(\log m)$). (We have chosen mass tracks that have a nearly constant logarithmic difference, but this normalization will correct for the small differences.) In Fig. 25, we show the run of log $\xi(\log m)$ with log m; the slope of this relation is the slope of the IMF, Γ, as given above. The error bars shown are those due to $\sqrt{N}$ counting statistics.

An (unweighted) least-squares linear fit gives a value for the slope $\Gamma = -1.8$. The formal error on this slope is 0.1 (it is clear from Fig. 25 that the fit is good), but it may assign too much weight to the high-mass bins, which contain only a few stars; however, the low-mass bin may be a little low due to possible incompleteness.

This value for the slope of the initial mass function is similar to those found for massive stars near the Sun, estimates of which range from $\Gamma = -1.3$ to -2.4 (Garmany, Conti, and Chiosi 1982; Scalo 1986; Lequeux 1979; Humphreys and McElroy 1984). Mateo (1988) studied a number of somewhat older LMC clusters, none of which contain stars as massive as those studied here; the average slope found by Mateo for stars with log $m > 0.45$ is 1.6–2.1, depending upon what assumptions are used.

We noted above that the number of stars with $M_{\rm bol} < -6$ (corresponding roughly to $15\mathcal{M}_\odot$) in LH 117 is about twice that in LH 118. We find from the numbers in Table XIII that this trend continues to lower masses.

TABLE XIII. The mass function of LH 117 and LH 118.

Mass Range	Number			$\xi(\log m)$
$\mathcal{M}_\odot$	LH117	LH118	Total	
60-90	1	0	1	0.65
40-60	1	1	2	1.3
25-40	4	2	6	3.3
15-25	10	4	14	7.2
9-15	36	21	57	29.
5-9	57	34	91	41.

TABLE XIV. Log number of Lyman photons ($cm^{-2}\ s^{-1}$).

Temp.	BB	Kurucz Models				Auer and Mihalas Models		
°K	log g =	3.5	4.0	4.5	5.0	3.3	4.0	4.5
20000	22.18	20.42	20.25	20.15	—	—	—	—
22500	22.62	21.18	20.97	20.84	—	—	—	—
25000	23.00	21.84	21.62	21.46	—	—	—	—
30000	23.55	23.05	22.78	22.62	—	23.30	22.55	22.17
35000	23.97	23.90	23.74	23.61	—	23.98	23.74	23.58
40000	24.30	—	24.23	24.18	24.14	24.33	24.21	24.15
45000	24.56	—	—	24.51	24.49	—	24.53	24.48
50000	24.79	—	—	24.76	24.74	—	24.77	24.73

c) The Hα Luminosity and the Lyman Continuum Flux

For distant galaxies, the integrated Hα luminosity is one of the main measures of recent star formation (e.g., Kennicutt 1983). The LMC offers an opportunity to compare the measured Hα fluxes with a known population of stars. Within a circular diameter of 6 arcmin Kennicutt and Hodge (1986) measure the Hα flux of DEM 323 to be 4×10^{-10} ergs $cm^{-2}\ s^{-1}$. With an assumed distance modulus of 18.3 and a correction for extinction $A_{H\alpha} = 0.2$, this implies a luminosity at Hα of 1.2×10^{38} ergs s^{-1}. This is about 30 times the Hα luminosity of the Orion Nebula (Kennicutt and Hodge 1986, and references therein), and implies a Lyman-continuum photon flux of $1.2\times10^{50}\ s^{-1}$.

We can compare this number with the predicted flux for the stars in the association. In Table XIV we present the flux of Lyman-continuum photons for various effective temperatures and gravities. The Kurucz (1979) models are LTE models of solar composition and include the effect of line blanketing. The Auer and Mihalas (1972) models are non-LTE models computed with zero metal abundances (hydrogen and helium only). As shown by Panagia (1973), Güsten and Mezger (1982), and Massey (1985), there is excellent agreement between the models and a blackbody approximation at the high temperatures characteristic of hot O stars. At lower temperatures, the blackbody model consistently predicts more Lyman photons than are predicted by either the line-blanketed or non-LTE models; however, most of the Lyman-continuum flux comes from the hottest stars. We have used our adopted temperatures and bolometric magnitudes to derive radii for the O stars in Tables VIII and IX, and computed the total number of ionizing photons per second for each star using the models of Table XIV. For LH 117 we find that the expected amount of ionizing radiation is $2.0\times10^{50}\ s^{-1}$ using the Kurucz models, and $2.5\times10^{50}\ s^{-1}$ using the higher fluxes predicted by the simple blackbody approximately. The majority of the radiation is contributed by the three early O type stars: $1.6\times10^{50}\ s^{-1}$. The Lyman photon flux from the stars in LH 118 (Table IX) is $3.3\text{–}5.5\times10^{49}\ s^{-1}$, about a factor of 5 lower than in LH 117, consistent with its lack of nebulosity compared to LH 117 (see Fig. 1).

The number of Lyman-continuum photons we expect based upon our stellar census of LH 117 is about a factor of 2 greater than what Kennicutt and Hodge (1986) detect from

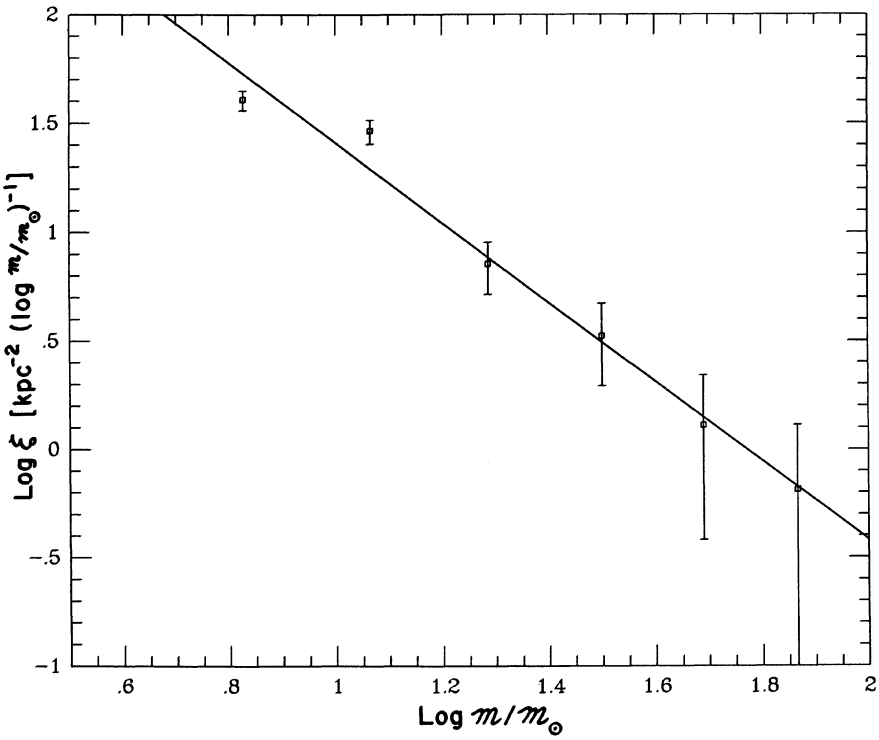

FIG. 25. Initial mass function of these two OB associations.

the Hα emission. Although this discrepancy is not severe, it is larger than that allowed by the 10%–15% errors of the Hα luminosity and what we estimate to be similar uncertainties in the determination of the Lyman-continuum fluxes. It may be that the H II region may be density bounded rather than radiation bounded. The H I maps of McGee and Milton (1966) show reasonably strong H I emission, at least along the line of sight. However, the CO map of Cohen *et al.* (1988) shows that LH 117 and LH 118 are on one edge of extended CO emission. This is reminiscent of "blister" H II regions, in which one side is density bounded and the other side is ionization bounded. It may also be that some of these Lyman photons are being absorbed by dust; although the average reddening is relatively low, the absorption does vary from star to star (see Table XI) and the Hα emission is patchy.

IV. SUMMARY AND CONCLUSIONS

We briefly summarize our results below:

LH 117 and LH 118 contain $\approx$50 stars with mass $> 10\mathscr{M}_\odot$. Of these, we have spectra for most of the stars with mass $> 15\mathscr{M}_\odot$, including two newly confirmed red supergiants.

Most of the stars in these two associations are in the first half of their lives on the main sequence. However, the two red supergiants and a B2 I star are of lower mass than several of the unevolved, more massive members of the associations, leading us to conclude that these supergiants must have formed ≈ 6–10×10^6 yr earlier than most of the association members.

The IMF of the associations has a slope of -1.8, similar to what is observed for massive stars near the Sun.

The Lyman-continuum flux should produce roughly twice the observed Hα flux, suggesting that the nebula is density bounded rather than radiation bounded.

We are grateful to Peter S. Conti for many useful discussions on this project, and to Taft Armandroff for several valuable suggestions. We also thank Ed Fitzpatrick for the use of his B type spectrum standards. This program would not have been possible without the generous support of observing time by the CTIO Director and TAC, and we thank the mountain staff for their continued excellent service over the years. Lisa Wells, Mario Hamuy, and Jeannette Barnes all aided in various stages of the data reduction, and we are, of course, grateful to Peter Stetson for providing us with DAOPHOT and his CCDCAL software. Carol Neese kindly commented on an early draft of this manuscript. Finally, we thank Myrna Cook and Joyce du Hamel of the Kitt Peak Photo Lab for their usual excellent technical support in the preparation of the illustrations. C.D.G. is partially supported by NSF grant no. AST 880-6594.

REFERENCES

Ardeberg, A., Brunet, J.-P., Maurice, E., and Prevot, L. (1972). Astron. Astrophys. Suppl. **6**, 249.
Auer, L. H., and Mihalas, D. (1972). Astrophys. J. Suppl. **24**, 193.
Blaauw, A. (1964). Annu. Rev. Astron. Astrophys. **2**, 213.
Bohannan, B., Abbott, D. C., Voels, S. A., and Hummer, D. G. (1986). Astrophys. J. **308**, 728.
Böhm-Vitense, E. (1981). Annu. Rev. Astron. Astrophys. **19**, 295.
Brunish, W. M., and Truran, J. W. (1982). Astrophys. J. Suppl. **49**, 447.
Cohen, R., Dane, T., Garay, G., Montani, J., Rubio, M., and Thaddeus, P. (1988). Astrophys. J. Lett. **331**, L95.
Conti, P. S., and Alschuler, W. R. (1971). Astrophys. J. **171**, 325.
Conti, P. S., Garmany, C. D., and Massey, P. (1986). Astron. J. **92**, 48.
Davies, R. D., Elliot, K. H., and Meaburn, J. (1976). Mem. R. Astron. Soc. **81**, 89.
Dufour, R. J. (1984). In *Structure and Evolution of the Magellanic Clouds*, IAU Symposium No. 108, edited by S. van den Bergh and K. S. de Boer (Reidel, Dordrecht), p. 353.
Elias, J. H., Frogel, J. A., and Humphreys, R. M. (1985). Astrophys. J. Suppl. **57**, 91.
FitzGerald, M. P. (1970). Astron. Astrophys. **4**, 234.
Flower, P., Geisler, D., Hodge, P., Olszewski, E., and Schommer, R. (1983). Astrophys. J. **275**, 15.
Flower, P. J. (1977). Astron. Astrophys. **54**, 31.
Garmany, C. D., Conti, P. S., and Chiosi, C. (1982). Astrophys. J. **263**, 777.
Garmany, C. D., Conti, P. S., and Massey, P. (1987). Astron. J. **93**, 1070.
Garmany, C. D., and Walborn, N. R. (1987). Publ. Astron. Soc. Pac. **99**, 240.
Garrison, R. F., Hiltner, W. A., and Schild, R. E. (1977). Astrophys. J. Suppl. **35**, 111.
Güsten, R., and Mezger, P. G. (1982). Vistas Astron. **26**, 159.
Herbst, W., and Miller, D. P. (1982). Astron. J. **87**, 1478.
Humphreys, R. M. (1979). Astrophys. J. Suppl. **39**, 389.
Humphreys, R. M., and McElroy, D. B. (1984). Astrophys. J. **284**, 565.
Humphreys, R. M., Nichols, M., and Massey, P. (1985). Astron. J. **90**, 101.
Jacoby, G. H., Hunter, D. A., and Christian, C. A. (1984). Astrophys. J. Suppl. **56**, 257.
Jaschek, C., and Jaschek, M. (1987). *The Classification of Stars* (Cambridge University, Cambridge).
Kennicutt, R. C. (1983). Astrophys. J. **272**, 54.
Kennicutt, R. C., and Hodge, P. W. (1986). Astrophys. J. **306**, 130.
King, I. R. (1971). Publ. Astron. Soc. Pac. **83**, 199.
Kormendy, J. (1973). Astron. J. **78**, 255.
Kudritzki, R. P., Simon, K. P., and Hamann, W.-R. (1983). Astron. Astrophys. **118**, 245.
Kurucz, R. L. (1979). Astrophys. J. Suppl. **40**, 1.
Landolt, A. U. (1983). Astron. J. **88**, 439.
Lequeux, J. (1979). Astron. Astrophys. **80**, 35.
Lequeux, J., Peimbert, M., Rayo, J. F., Serrano, A., and Torres-Peimbert, S. (1979). Astron. Astrophys. **80**, 155.
Lucke, P. (1972). Ph. D. thesis, University of Washington.
Lucke, P. B., and Hodge, P. W. (1970). Astron. J. **75**, 171.
Maeder, A. (1988). Astron. Astrophys. (in press).
Maeder, A., and Meynet, G. (1987). Astron. Astrophys. **182**, 243.
Massey, P. (1985). Publ. Astron. Soc. Pac. **97**, 5.
Massey, P., Jacoby, G., and Neese, C. (1987). NOAO Newsl. No. 11, p. 20.
Mateo, M. (1988). Astrophys. J. **331**, 261.
McGee, R., and Milton, J. (1966). Aust. J. Phys. **19**, 343.
Panagia, N. (1973). Astron. J. **78**, 929.
Ratnatunga, K. U., and Bahcall, J. N. (1985). Astrophys. J. Suppl. **59**, 63.
Sanduleak, N. (1969). Contrib. Cerro Tololo Inter-American Obs. **89**.
Sanduleak, N., and Philip, A. G. D. (1977). Publ. Warner and Swasey Obs. **2**, 105.
Scalo, J. M. (1986). Fundam. Cosmic Phys. **11**, 1.
Simon, K. P., Jonas, G., Kudritzki, R. P., and Raha, J. (1983). Astron. Astrophys. **125**, 34.
Stetson, P. B. (1987). Publ. Astron. Soc. Pac. **99**, 191.
Tinsley, B. M. (1980). Fundam. Cosmic Phys. **5**, 287.
Van de Hulst, H. C. (1952). In *The Atmospheres of the Earth and Planets*, edited by G. P. Kuiper (University of Chicago, Chicago), p. 49.
Voels, S. A., Bohannan, B., Abbott, D. C., and Hommer, D. G. (1988). Astrophys. J. (in press).
Walker, A. (1988). NOAO Newsl. No. 13, p. 20.

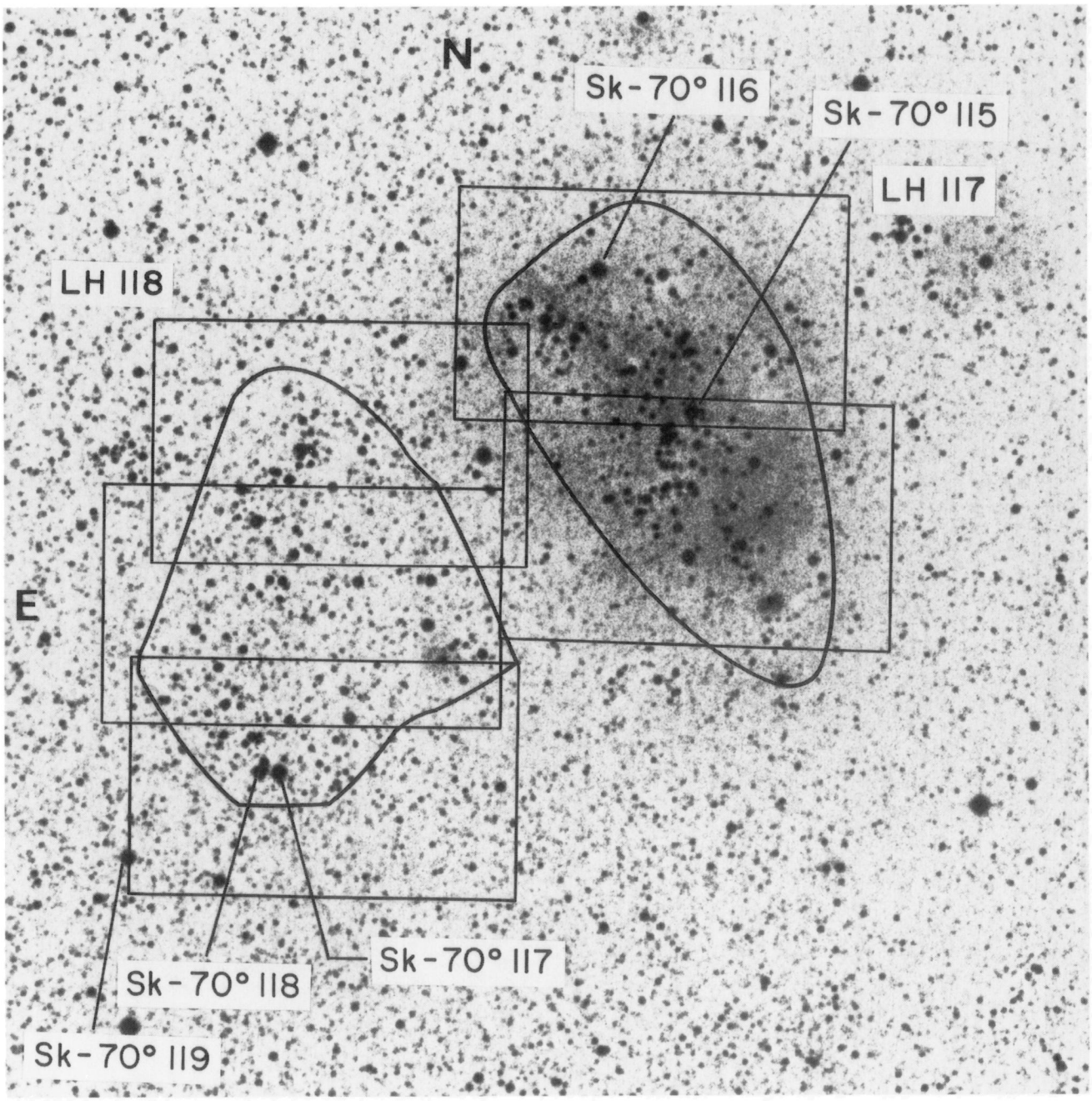

FIG. 1. Enlargement of the ESO "Quick Blue" Survey plate 057. The location of the five *UBV* CCD frames (Table I) is shown, along with the identification of the Sanduleak (1969) stars.

Massey *et al.* (see page 110)

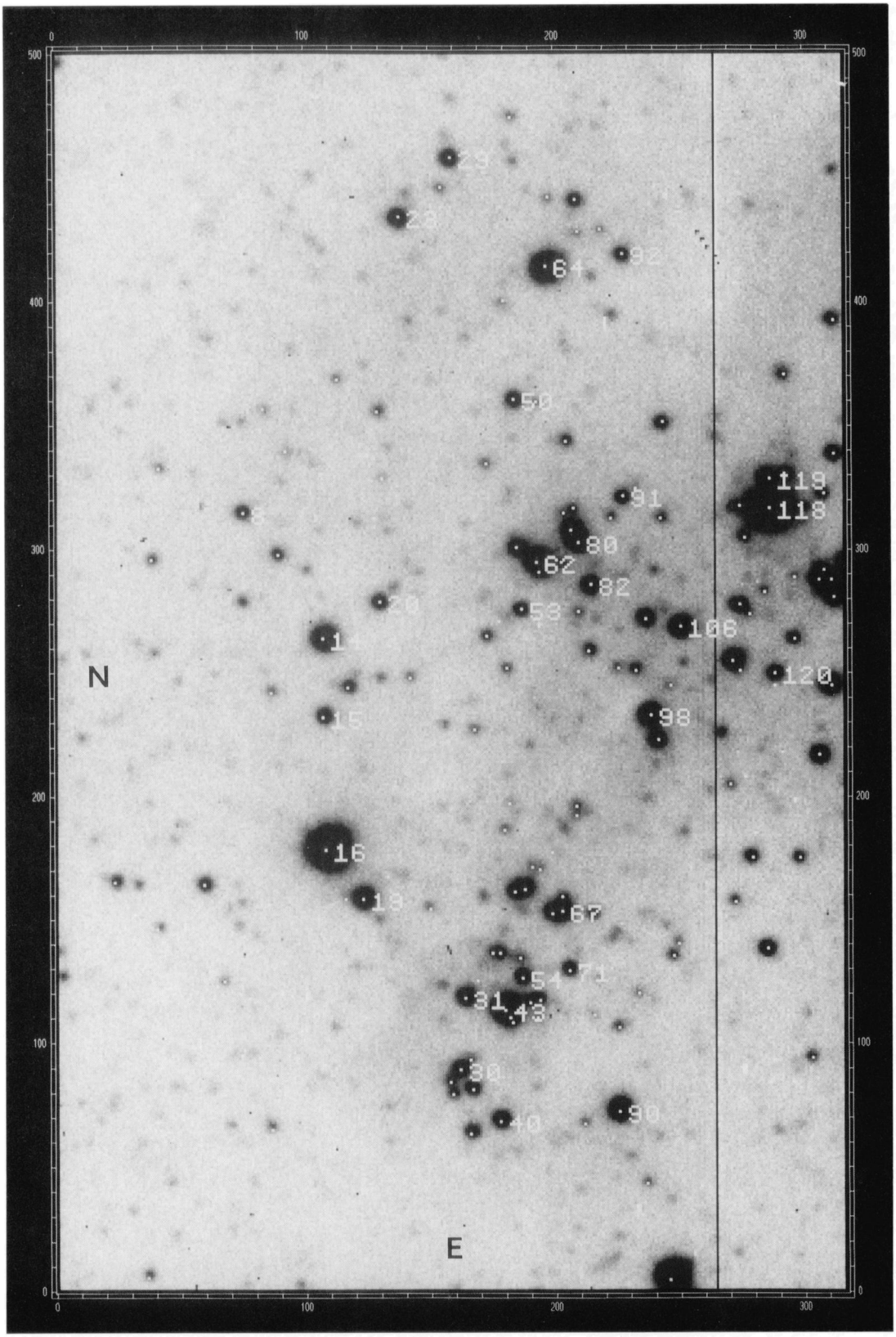

FIG. 2. Field LH 117N. The location of all stars with photometry is shown by dots in the "northern" field of LH 117. The brighter, less crowded stars are shown with their numbers from Table IV. The frame shown is the long *B* exposure. The *x*,*y* values for stars 1–128 in Table IV can be used with this figure.

Massey *et al.* (see page 110)

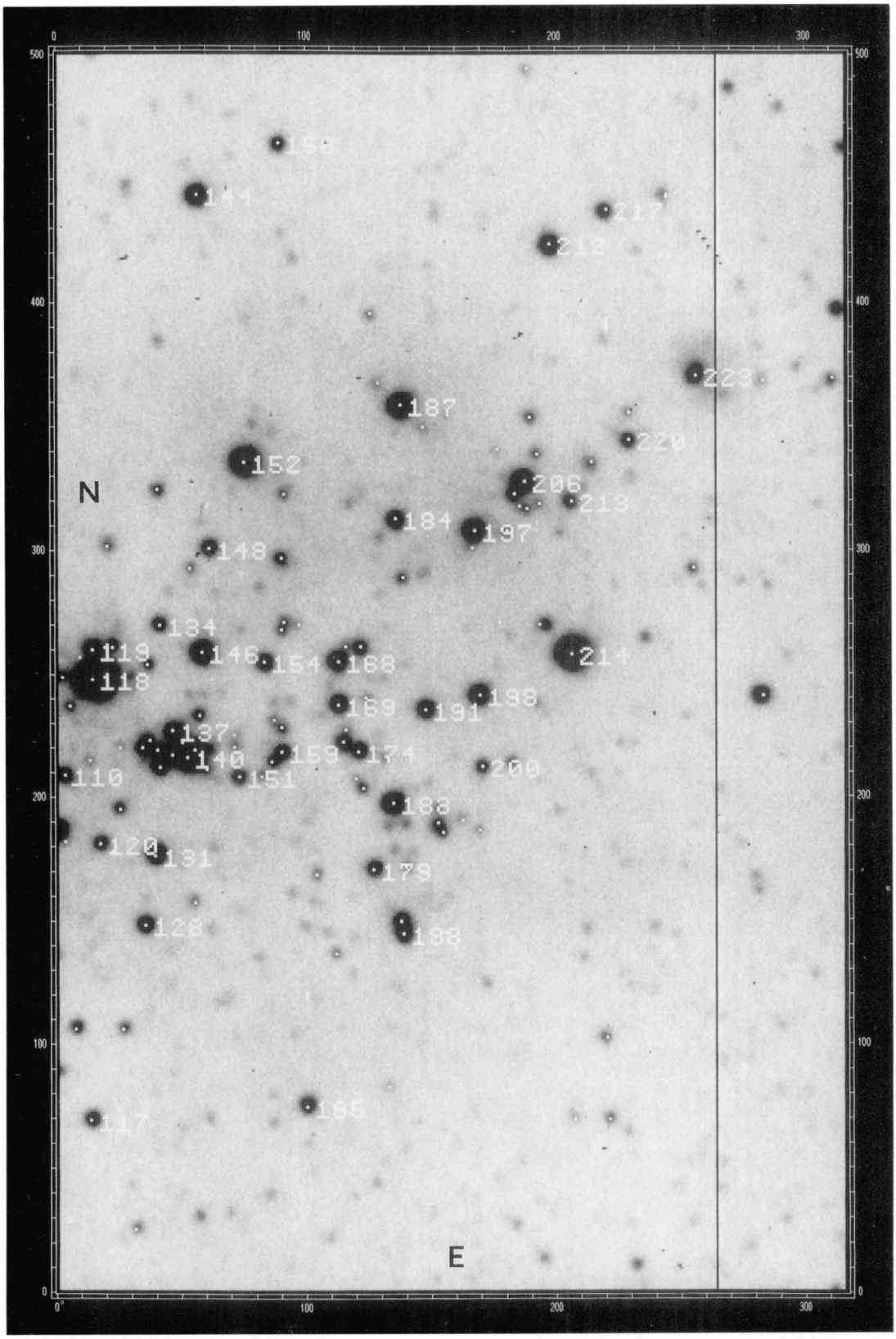

FIG. 3. Field LH 117S. Same as Fig. 2, but for the "southern" field of LH 117. The *x,y* values for stars 129–235 in Table IV can be used with this figure.

Massey *et al.* (see page 110)

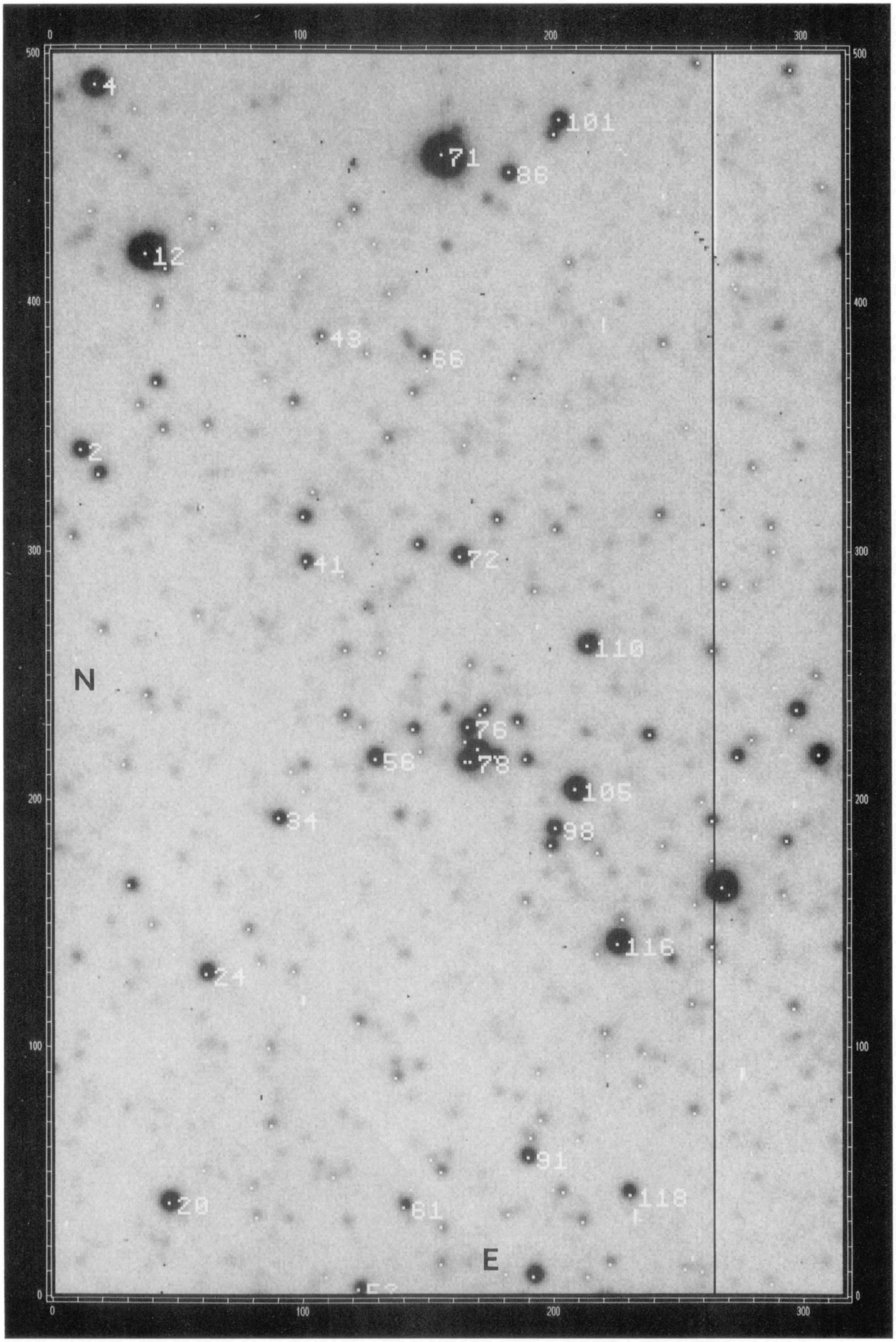

FIG. 4. Field LH 118N. Same as Fig. 2, but for the "northern" field of LH 118. The *x,y* values for stars 1–152 in Table V can be used with this figure.

Massey *et al.* (see page 110)

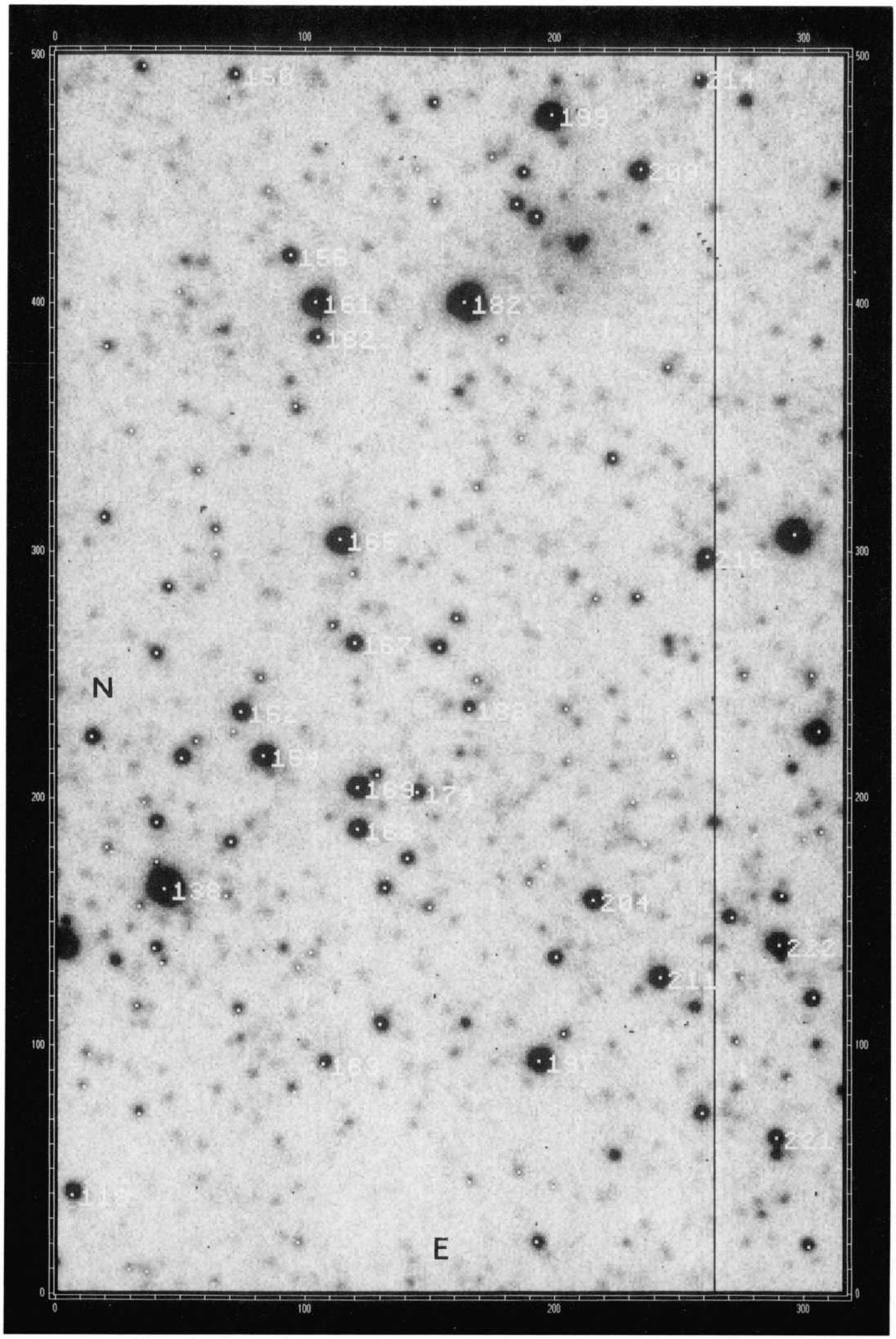

FIG. 5. Field LH 118S. Same as Fig. 2, but for the "southern" field of LH 118. The *x,y* values for stars 153–226 in Table V can be used with this figure.

Massey *et al.* (see page 110)

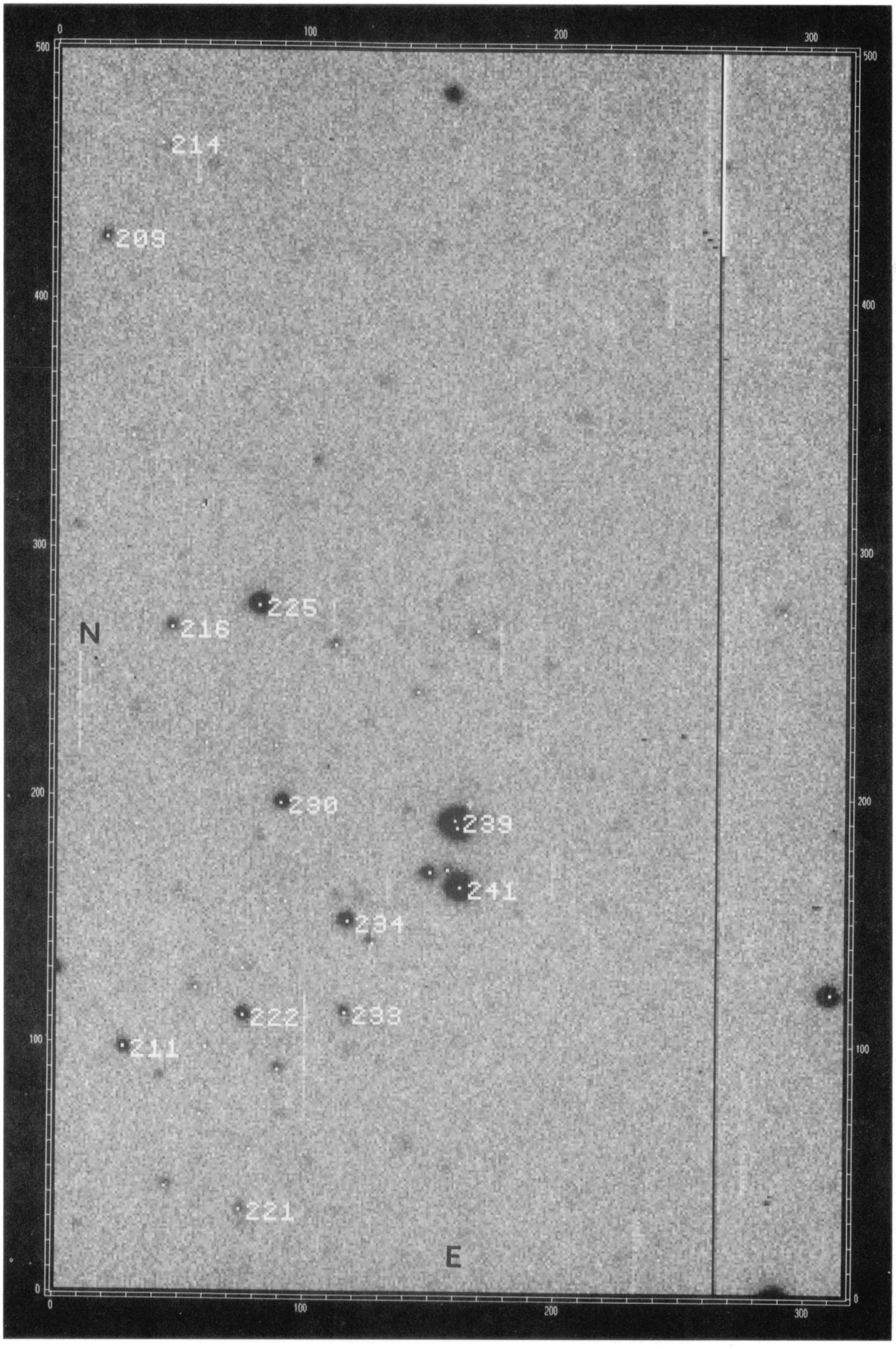

FIG. 6. Field LH 118X. Same as Fig. 2, but for the "extra" frame of LH 118, located to the south of Fig. 4. The *x,y* values for stars 227–224 can be used with this figure.

Massey *et al.* (see page 110)

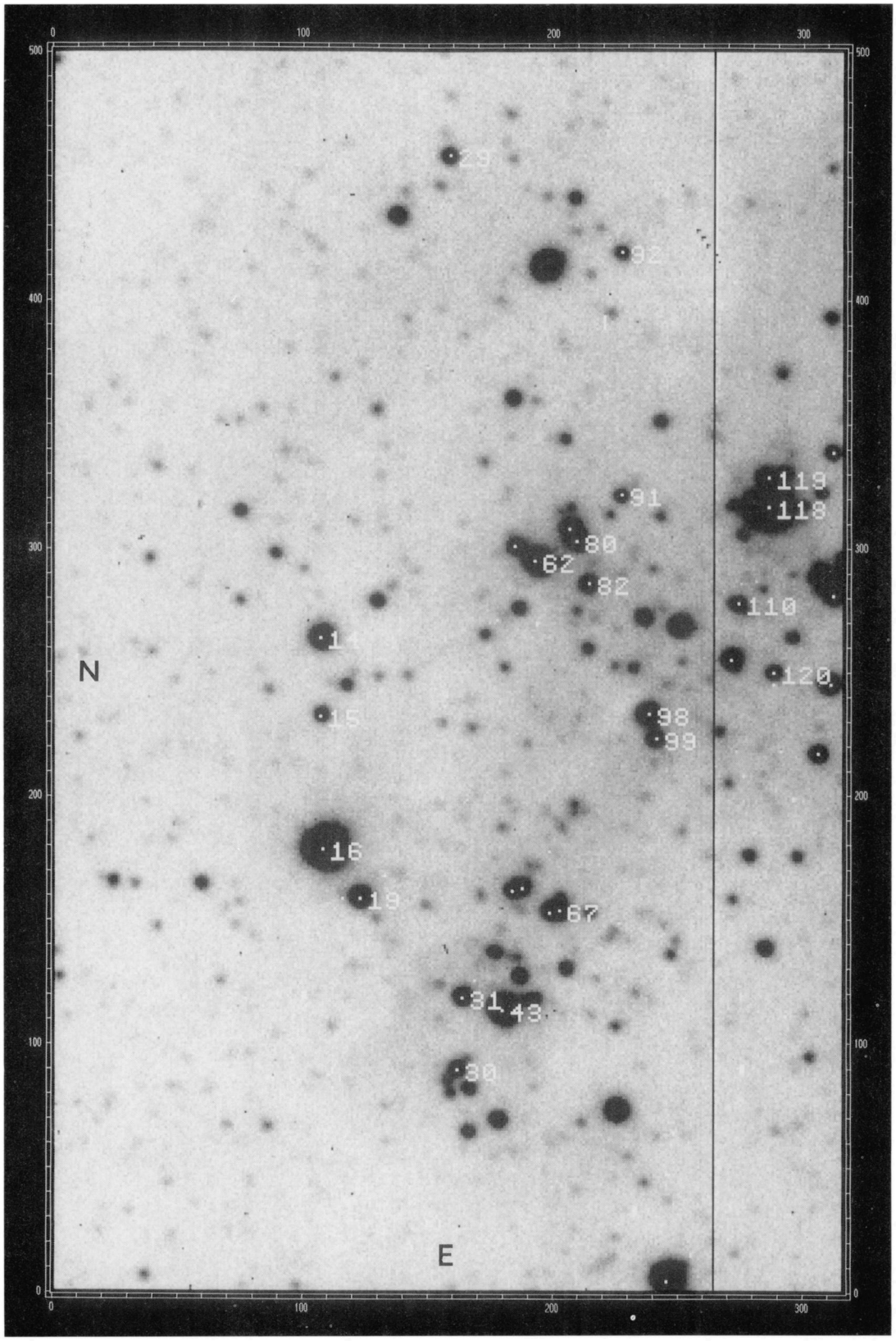

FIG. 10. Finding chart for the bluest stars in LH 117N. The stars in Table VIII with numbers 128 or less can be found on this chart.

Massey *et al.* (see page 116)

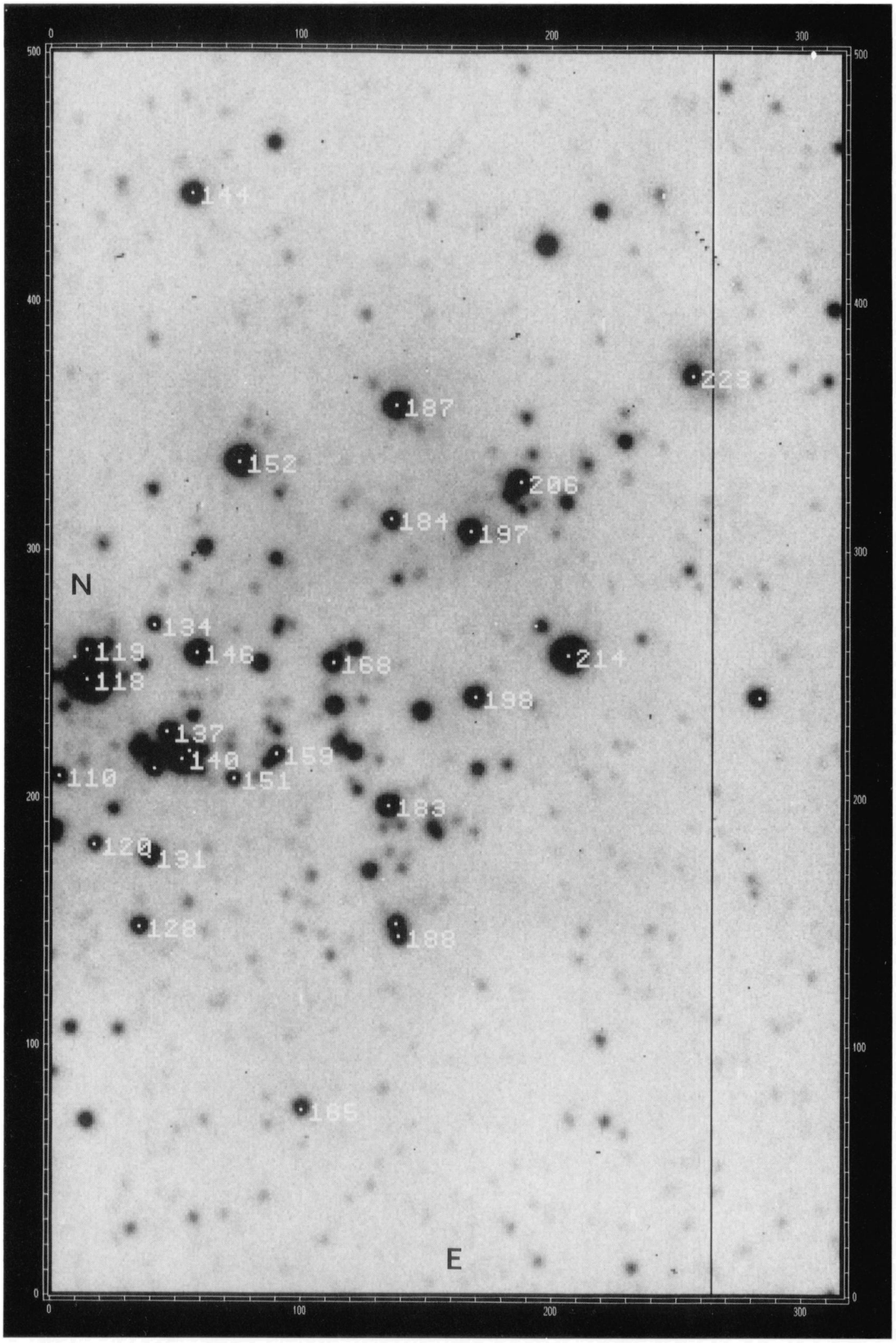

FIG. 11. Finding chart for the bluest stars in LH 117S. The stars in Table VIII with numbers 129 or greater can be found on this chart.

Massey *et al.* (see page 116)

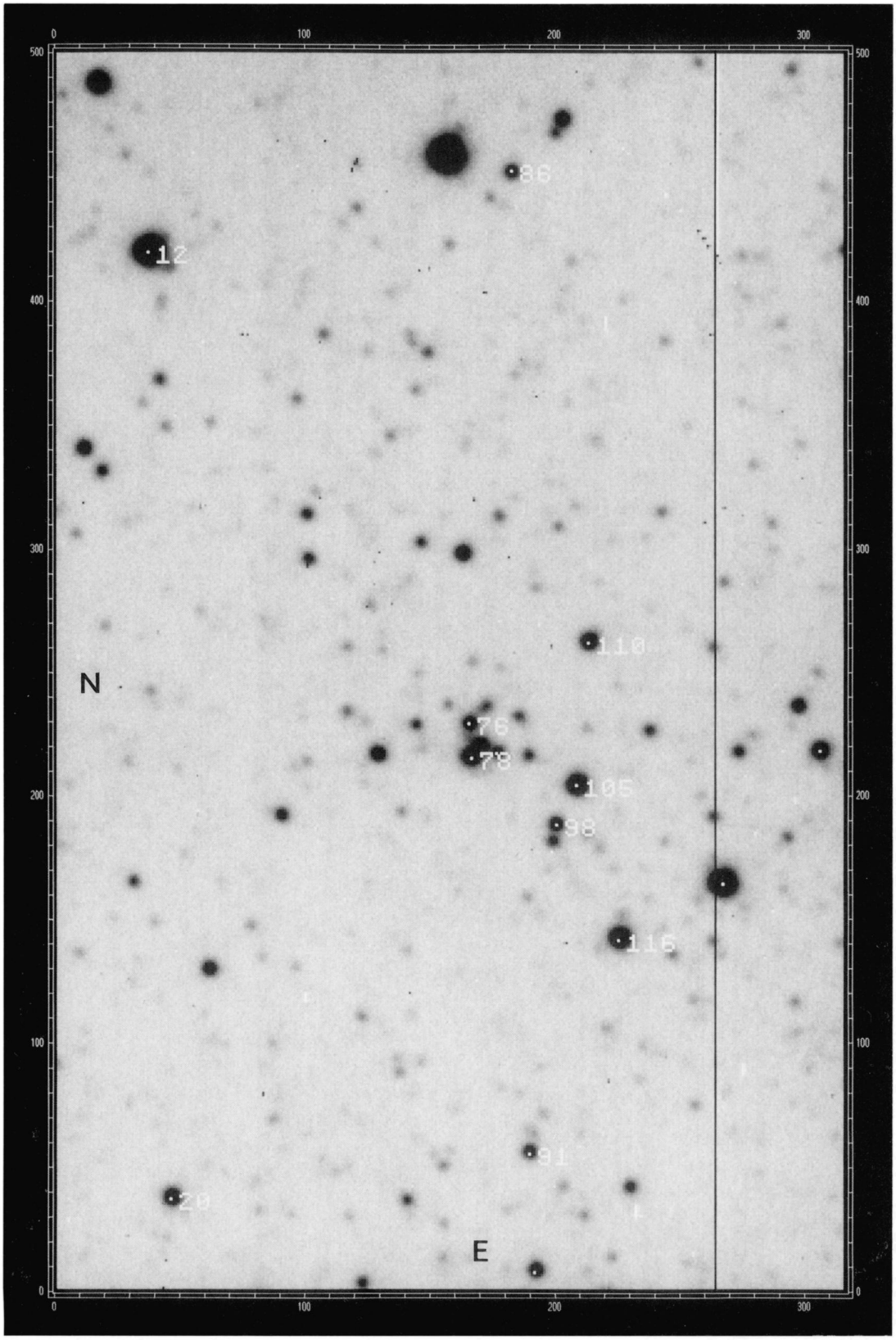

FIG. 12. Finding chart for the bluest stars in LH 118N. The stars in Table IX with numbers 152 or less can be found on this chart.

Massey *et al.* (see page 116)

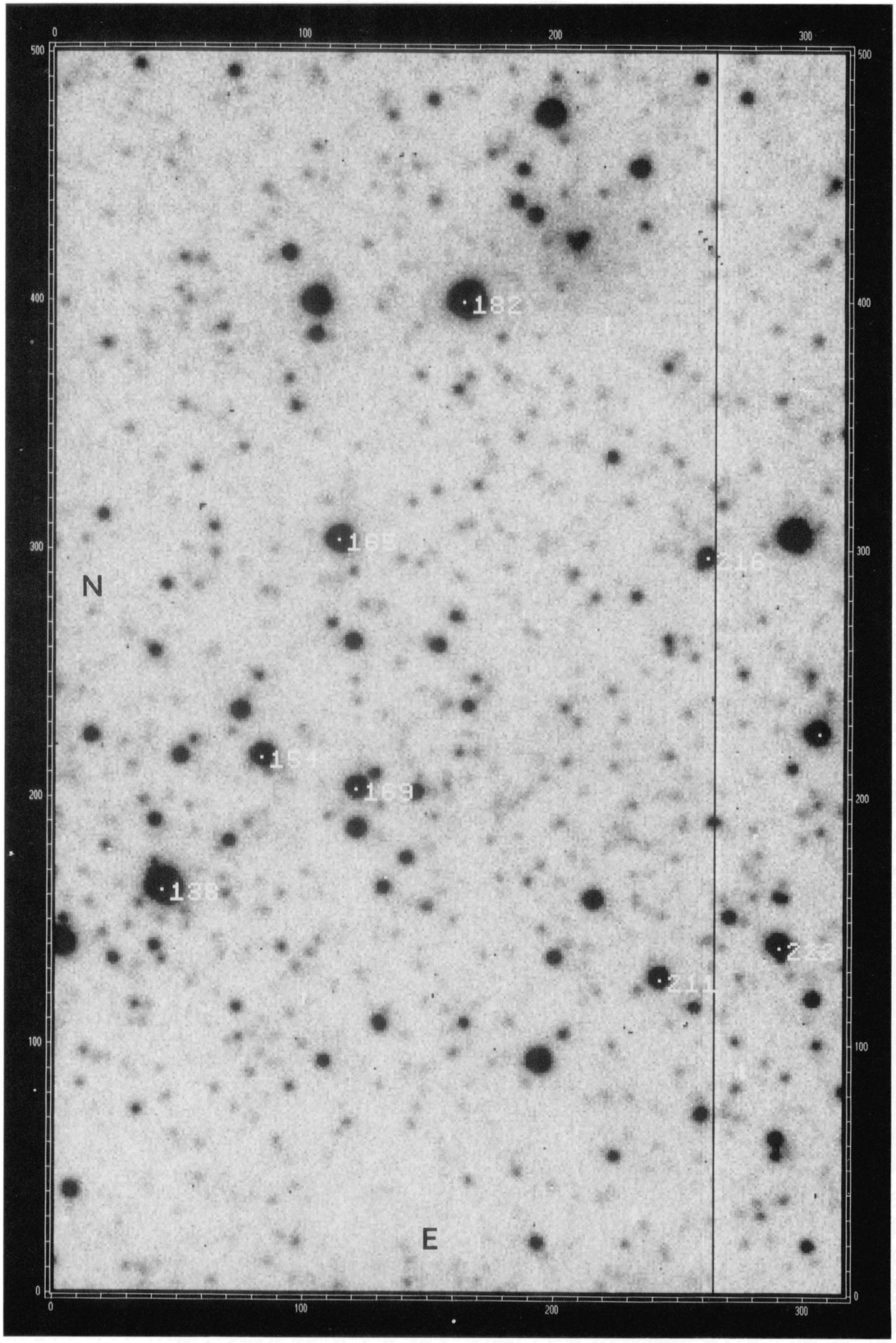

FIG. 13. Finding chart for the bluest stars in LH 118S. The stars in Table IX with numbers between 153 and 226 can be found on this chart.

Massey *et al.* (see page 116)

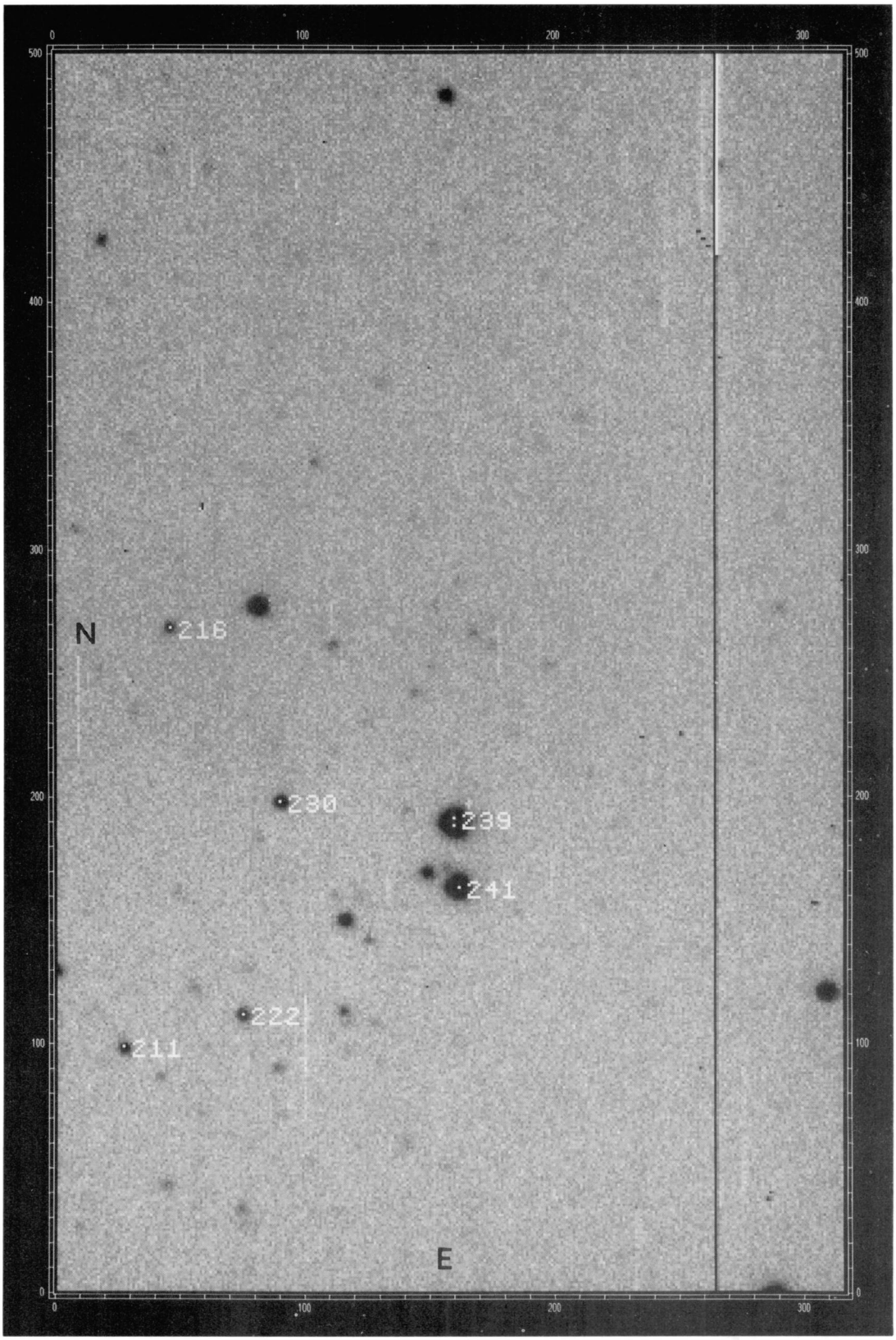

FIG. 14. Finding chart for the bluest stars in LH 118X. The stars in Table IX with numbers 227 or greater can be found on this chart.

Massey *et al.* (see page 116)

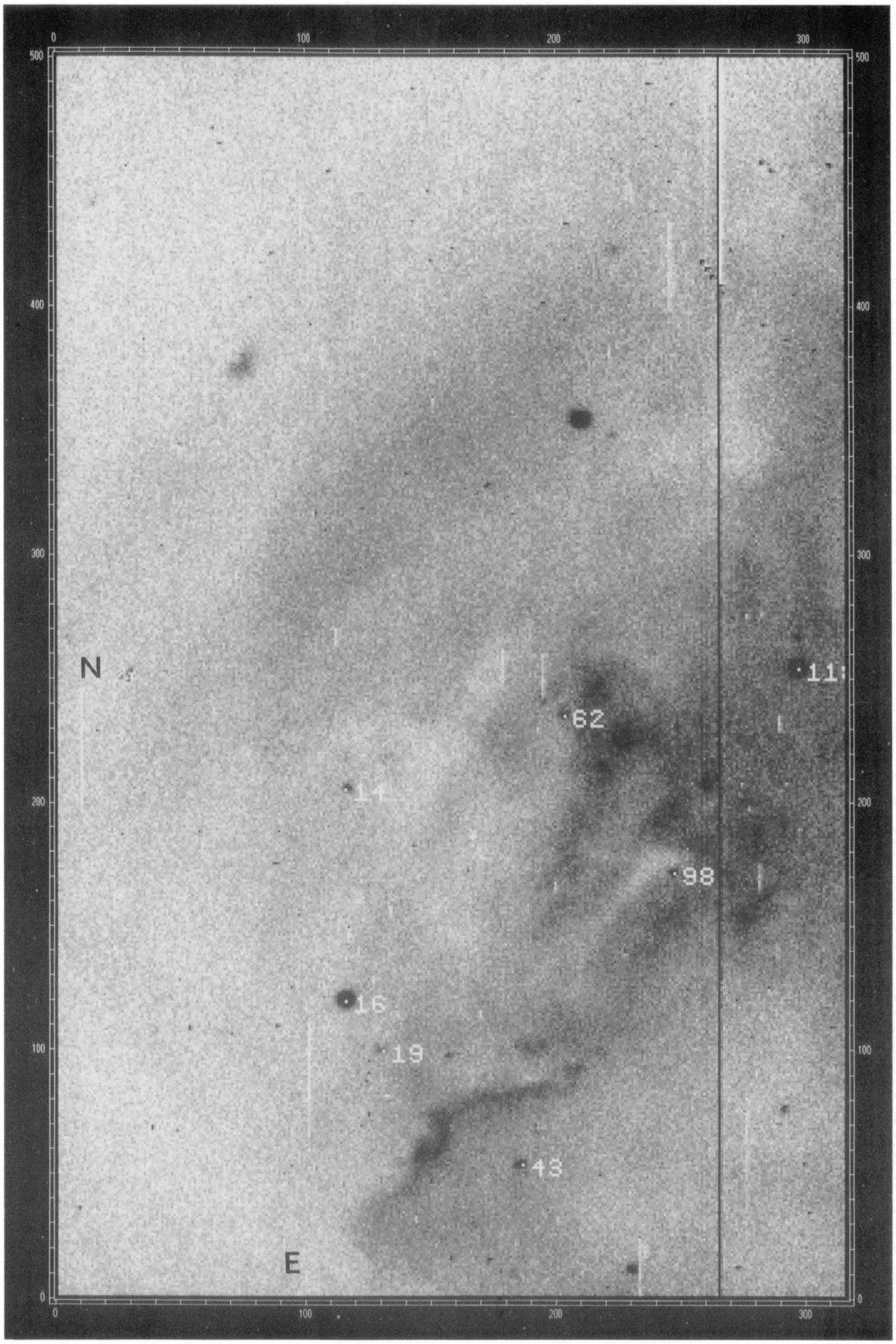

FIG. 15. An Hα frame of LH 117N. A few of the bright blue stars are indicated.

Massey *et al.* (see page 116)

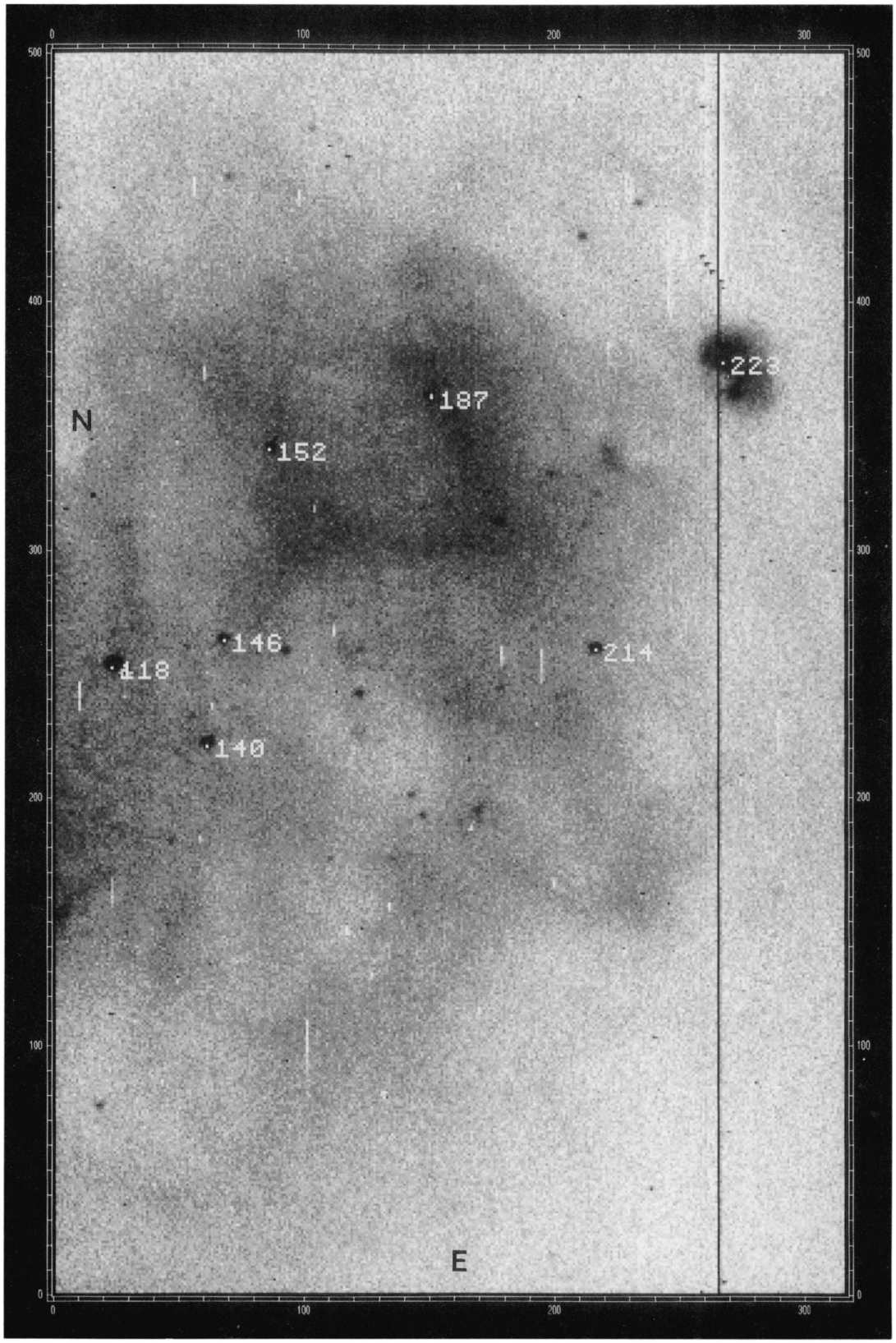

FIG. 16. An Hα frame of LH 117S. A few of the bright blue stars are indicated.

Massey *et al.* (see page 116)